

The rapid emplacement of the 1823 CE Keaīwa lava flow from the Great Crack in the Southwest Rift Zone of Kīlauea volcano

A THESIS SUBMITTED TO THE GRADUATE DIVISION OF THE UNIVERSITY OF HAWAII AT MĀNOA IN PARTIAL FULFILLMENT OF THE REQUIREMENTS FOR THE DEGREE OF

MASTER OF SCIENCE
IN
EARTH AND PLANETARY SCIENCES

JULY 2024

By

Andrea Belen Tonato Nacato

Thesis Committee:
Tom Shea, Chairperson
Garrett Apuzen-Ito
Helen Janiszweski

Keywords: SWRZ, fissure, lava flow, modeling, effusion rate

Table of contents

CHAPTER 1	1
Abstract	1
Introduction	2
Geological Background.....	3
Southwest Rift Zone	3
Southwest Rift Zone Eruptive Record.....	4
1823 CE Eruption and Great Crack.....	5
Methods.....	7
Fieldwork and Sample Collection	7
Chemistry.....	8
Radiocarbon Dating.....	9
Modeling.....	9
Results	9
Field Observations and Measurements.....	9
Petrographic Characteristics	12
Chemistry.....	12
VolcFlow Modeling.....	16
Discussion	21
Formation of the Great Crack.....	21
Magma Source	23
Emplacement Rate and Lava Flow Velocity	23
Conclusions	23
Acknowledgements	24
CHAPTER 2	25
Introduction	25
Dike Propagation	25
Caldera Collapse.....	26
Methods.....	28
Dike propagation	28
Caldera Collapse.....	29
Results	30
Dike Propagation	30

Caldera Collapse.....	31
Conclusion.....	32
Acknowledgments.....	33
References cited	33

Table of figures

Fig. 1. Location of Kīlauea volcano (inset map) and lava flows within the Southwest Rift Zone that erupted from post-1790 CE to its most recent eruption in December 1974 (modified from Sherrod et al., 2021). For reference the recent eruptions (2020–23) within Halema‘uma‘u Crater are shown, as is the 1 m isopach of the ~1500 to early 1800s Keanakāko‘i Tephra (Swanson et al., 2014; Swanson and Houghton, 2019).....	4
Fig. 2. Map showing the study area and an aerial view of a small portion of the fissure called the Great Crack. Included are the locations of field measurements and collected samples.	6
Fig. 3. Lava Plastered Cones. A) The photo shows the northernmost Lava plastered cones surrounded by the 1823 lava flow, yellow arrows show the direction of the flow perpendicular to the cones alignment, and B) shows the tallest cone covered by the 1823 lava flow.	7
Fig. 4. The sketch shows the criteria used to measure tree molds.	10
Fig. 5. Photos showing volcanic features that interacted with the 1823 CE lava flow. A) pāhoehoe-like sheet flow, B) 1823 lava flow thickness at the inner wall of the Great Crack, C) transitional lavas that cover a transitional area between A and B, D) lava drain-back features that cover lava balls and the fissure part of the Great Crack, E) sequences of lava balls along the fissure wall, F) ramp-up of 1823 CE lava that covers a pre-existing tumuli, G) Kīpuka of older lava that has been partially overrun and surrounded by the 1823 CE lava flow, and H) tree molds with charred wood and one that is hollow.....	11
Fig. 6. Comparison of the Forsterite percentage of the Keaīwa lava flow and Keala‘alea hills compared with other Kīlauea eruptions that occurred around the same period of time at the summit and SWRZ. The symbols are larger than the analytical errors for the data (Fo from the Great Crack). Chemical data shown for comparison are from Garcia et al. (2003), Lynn et al. (2017), Lynn and Swanson (2022) and Downs et al. (2023).....	13
Fig. 7. Plot shows a comparison of Olivine Forsterite vs NiO among other eruption of Kīlauea that occurred during the same period of time. The symbols are larger than the analytical errors for the data (Fo from the Great Crack). Chemical data shown for comparison are from Garcia et al. (2003), Lynn et al. (2017), Lynn and Swanson (2022) and Downs et al. (2023).....	14
Fig. 8. The plots show the results of bulk rock analyses from the Keaīwa lava flow and Keala‘alea hills compared with other Kīlauea eruptions that occurred around the same period of time at the summit and SWRZ. The symbols are larger than the analytical errors for the data. Chemical data shown for comparison are from Garcia et al. (2003), Lynn et al. (2017), Lynn and Swanson (2022) and Downs et al. (2023).....	15
Fig. 9. Comparison between thicknesses obtained from VolcFlow and thicknesses measured in the field.....	16
Fig. 10. Results from lava flow modeling. Linear relationship between time vs volume show the minimum effusion rate (boundary between the squares and the triangles) required for the lava flow to cover the Lava Plastered Cones.	17
Fig. 11. Lava Plastered Cones in VolcFlow. The 2 m DEM’s show the criteria used to classify the models. White squares show the area used to classified wheter the flow is succesful or not. Black arrows show flow direction.	18
Fig. 12. Effusion rate required to cover a flow field area. Effusion rates behave consistent for volumes $\geq 5\,000\,000\text{ m}^3$	19
Fig. 13. Maximum velocity reached when the lava flow reaches the Lava Plastered Cones.....	19
Fig. 14. The complete extent of the VolcFlow simulation for the 1823 CE eruption. It shows a good fit of the simulation within the actual flow field outline. Black lines are topographic contour lines.	20
Fig. 15. The plot shows a comparison between the VolcFlow model results and other eruptions that occurred worldwide in terms of effusion rate vs time. The black arrow shows the tendency of the VolcFlow models in time. Eruption rates shown for comparison are from (Acocella & Neri, 2009; Andronico & Lodato, 2005;	

Calvari et al., 1994; Coltelli et al., 2007; Coppola et al., 2017; Dietterich et al., 2021; Favalli et al., 2006; Harris & Neri, 2002; Lipman & Banks, 1987; Staudacher et al., 2009; Tazieff, 1977; Vicari et al., 2007)	21
Fig. 16. Great Crack where it breaks the Kealaalea Hills lava flow – erupted less than 33 years prior - that shows no syn-eruptive widening or drain-back features. Also shows that the Great Crack is not as deep in the northern portion as it is down to the southwest.	22
Fig. 17. The image A shows how dike propagates from a source, and B shown how a dike looks like in nature (Taken from Maßmeyer et al., 2013).	26
Fig. 18. Caldera collapse during the Pu‘u‘O‘o eruption in 2018. Photos show a deformation of the Halema‘uma‘u crater at the summit of Kīlauea volcano. Photographs belong to the U. S. Geological Survey.	27
Fig. 19. Main materials used in the setup of the analog model for dike propagation.	28
Fig. 20. Dimension of the tank made of plexy glass showing the hole at the base of the container.	28
Fig. 21. Gelatin after 24 hours. It shows how to add the layer of flour, and where to place the polarized sheets.	29
Fig. 22. Image shows dimensions and every item used to build the set up of the caldera collapse model.	30
Fig. 23. The set of photos show two layers of gelatin that diffused, and impede to clearly see the intrusion of colored water.	30
Fig. 24. Differences between using water with food coloring, and water with acrylic paint.	31
Fig. 25. Sequence of photos show (from left to right) the faucets of the system closed, while red water is being injected creating radial cracks at the summit of the modeled volcano.	32
Fig. 26. From right to left, the photos show the red water flowing down from the tube system creating a caldera collapse at summit of the volcano.	32

CHAPTER 1

The rapid emplacement of the 1823 CE Keaīwa lava flow from the Great Crack in the Southwest Rift Zone of Kīlauea volcano

Andrea Tonato^{1*}, Thomas Shea¹, Drew T. Downs², and Karim Kelfoun³

¹ SOEST, University of Hawai‘i at Mānoa, Honolulu HI, USA

² U.S. Geological Survey, Hawaiian Volcano Observatory, Hilo, HI 96720, USA

³ Laboratoire Magmas et Volcans, Université Clermont Auvergne, Clermont-Ferrand, France

*Corresponding author

Abstract

The 1823 CE Keaīwa lava flow in the Southwest Rift Zone (SWRZ) of Kīlauea volcano is unique for its expansive pāhoehoe sheet flow morphology and lack of constructive vent topography, despite having a similar tholeiitic basalt composition to other lavas erupted from Kīlauea. This lava flow issued from a ~10 km-long continuous fissure known as the Great Crack, and has an unusually thin sheet flow-like morphology with margin thicknesses of ~15–110 cm (average of 42 cm). Based on field observations of the lava flow at its fissure vent (e.g., drain-back features), we propose that the Great Crack formed, or at least significantly widened, syn-eruptively during the 1823 CE eruption. The absence of pyroclastic or scoria cones indicates that the eruption consisted of a rapid outpouring of relatively degassed lava as the fissure unzipped. This rapidly moving lava flow overtopped pre-existing tumuli and scoria cones (e.g., Lava Plastered Cones) up to ~10 m tall. Glass and whole-rock chemistry yield homogeneous compositions for the lavas erupted from the Great Crack, with glass compositions of 6.40 ± 0.10 wt. % and whole-rock compositions of 7.39 ± 0.07 wt. % MgO. A shorter western fissure system is richer in mafic minerals (e.g., olivine and clinopyroxene), and therefore the lavas from this fissure are slightly more MgO-rich (7.79 ± 0.05 wt. %). MgO-in-glass thermometry was used to calculate eruption temperatures of $1153 \pm 13^\circ\text{C}$ from spatter from the Great Crack fissure. These temperatures are typical of Kīlauea lavas, thus the extensive sheet-like lava flow morphology is not a direct consequence of unusual magmatic or rheological conditions (i.e. low viscosity). Instead the flow morphology is associated with high effusion rates caused by sudden drainage of uplift magma through the Great Crack. Lava flow modeling using VolcFlow on a 2 m DEM indicates that a minimum bulk effusion rate of ~11,200 m³/s (~6,700 m³/s dense rock equivalent, assuming ~40 % vesicularity) and a minimum flow velocity of ~11 m/s are required for the lava to overcome the Lava Plastered Cones. These effusion rates are amongst the highest inferred for eruptions in Hawai‘i. This study sheds light on an anomalous eruption style that occurred from the unique fissure that is the Great Crack and the dynamics involved in its lava flow emplacement; providing new insights into potential risks and hazards during basaltic eruptions from Kīlauea and possibly Mauna Loa. An eruption similar to 1823 CE with a time frame shorter than an hour, high effusion rates, and rapid flow front velocities would not easily allow for evacuation.

Introduction

Lava flow morphology is intimately linked with the physics of lava emplacement. Lava flow geometries, internal structures, and surface morphology record intrinsic (e.g., composition, temperature, crystallinity) and extrinsic (e.g., topography, effusion rate, flow velocity) parameters that operate during emplacement (i.e., Cashman et al., 1999; Harris and Rowland, 2015). Quantifying these parameters is useful in the case of eruptions that were not witnessed or monitored firsthand, particularly as flow morphologies are useful indicators of emplacement characteristics that can help characterize lava flow hazards at frequently active volcanoes. Kīlauea is one such frequently active shield volcano on the Island of Hawai‘i that is dominated by eruptions of tholeiitic basalt. Effusive lavas erupted from Kīlauea have variable flow morphologies that include pāhoehoe and its sub-types (e.g., toothpaste, sheet, slaby, shelly) and ‘a‘ā lavas (Holcomb, 1987; Walker, 1999; Harris and Rowland, 2015).

Pāhoehoe lava flows commonly have smooth, hummocky surfaces, and can be as thin as a few centimeters upon initial emplacement before reaching several meters thick after repeated breakouts and inflation (Macdonald, 1953; Rowland and Walker, 1987; Harris and Rowland, 2015). These flows initially propagate as lobes of lava forming a thin crust that act as an insulator and retainer to incoming lava from upslope. This process forms pāhoehoe toes at their flow fronts. The internal pressure of lava deforms the skin plastically, allowing the toe to swell before rupturing to form a newer toe (Hon et al., 1994; Cashman et al., 1999). This repeated process leads to the formation of complex flow fields with networks of tubes, frontal lobes, and toes. Pāhoehoe lava flows are thus commonly compound flows that accumulate generations of branching tubes, breakouts, and sub-units (Mattox et al., 1993). They are considered the morphological hallmark of low viscosities and effusion rates (Rowland & Walker, 1990; Cassidy et al., 2018). ‘A‘ā lava flows on the other hand have a rough, auto-brecciated surface covered by clinker (Harris and Rowland, 2015). ‘A‘ā flows typically range from 0.5 to 20 m thick, and are characterized by a core sandwiched between two layers of variably thick clinker or breccia. While ‘a‘ā flows can initially propagate as a simple sheet-like unit, the velocity difference causes formation of more central channels and stalling along flow edges (Harris and Rowland, 2015).

Extensive pāhoehoe sheet flows, defined as simple flows consisting of one, or a few extensive but thin sheets, emplaced within a short time frame, are less common at Kīlauea. Their surface is still smooth, but much less dominated by intricate, ropy surfaces traditional of slowly advancing pāhoehoe flows. Observed instances of active sheet flows during the 1969–71 Maunaulu or 1983–2018 Pu‘u‘ō‘ō eruptive phases were emplaced close to their vents, at locally high effusion rates and velocities. These sheet flows only extended a few hundred meters from their vents (Swanson, 1973; Mattox et al., 1993). A more extensive, several kilometer-long pāhoehoe sheet flow formed at Krafla (Iceland) in 1984 during its initial high effusion phase (Rossi, 1997), but observed instances are otherwise scarce.

Here, we investigate the 1823 CE Keaīwa lava flow from the Great Crack in the lower Southwest Rift Zone (SWRZ) of Kīlauea volcano. The lava flow produced during this eruption is anomalous compared to others from Kīlauea in that it is comprised of an unusually thin (typically <1 m), several kilometers-long sheet flow morphology that has a pāhoehoe-like proximal surface and more distal ‘a‘ā lava morphologies. This lava erupted along a remarkably continuous and extensive fissure called the Great Crack that lacks any constructional vent features (e.g., scoria cones, spatter ramparts). Stearns (1926) was the first to conduct a detailed study of this lava flow, and noted it as being unique when he stated ‘Although similar, perhaps, in texture and composition to some other flows, it is unusual because of its source, the manner of its extrusion, and its

thinness.’ Additionally, the anomalous behavior of this flow is recorded in the fact that it overtopped a set of pre-existing cones called the Lava Plastered Cones, the tallest of which stands ~10 m above the surrounding lava plain (Stearns, 1926; Soule et al., 2003). Overtopping of this topography is thought to indicate either rapid flow and high effusion rates or ponding against the cones and drainage (Stearns, 1926; Baloga et al., 1995; Guest et al., 1995; Soule et al., 2003).

We conducted fieldwork to obtain measurements to constraints on the near vent and more distal flow features. We measured lava flow thicknesses at the fissure, kipukas, margins, tree molds, and at ramp-up features. Petrographic and geochemical characterization of samples from this eruption were undertaken to determine if this lava is rheologically anomalous compared to other tholeiitic basalts at Kīlauea. These data were combined to provide realistic input parameters for VolcFlow modeling to better understand the effusion rate and velocities. Specifically, we aimed to tackle the following questions: (1) What caused this eruption? Was the rift system overpressurized or responding to an extensional rift opening event? (2) Did the Great Crack form during the 1823 CE eruption, and if so, what does the lack of constructional vent features indicate about the style and underlying cause for the eruption? (3) Did the lava flow pond against or override the Lava Plastered Cones, and what does this imply for emplacement velocity? (4) Given the new field, geochemical, rheological, and numerical modeling constraints, what are plausible ranges in effusion rates and emplacement timescales for large scale sheet flows at Kīlauea?

Geological Background

Southwest Rift Zone

About 90% of Kīlauea’s surface area is covered by lava flows younger than 1,500 years old as a result of its high eruption frequency (Sherrod et al., 2021). This is a reflection of the high magma supply of the Hawaiian hotspot that feeds Kīlauea’s magma reservoirs at a rate of at least 0.1 km³/yr (Poland et al., 2014). The summit region of Kīlauea currently hosts two long-lived magma reservoirs; the deeper and larger South Caldera reservoir at 3–5 km depth with an estimated volume of 3–20 km³, and the shallower Halema‘uma‘u reservoir at 1–2 km beneath Halema‘uma‘u Crater with estimated volumes of 0.2–8 km³ (Poland et al., 2014; Anderson et al., 2019). These reservoirs supply magma to the summit as well as to the two rift zones that radiate from the summit: the East Rift Zone (ERZ) and SWRZ. The ERZ is ~130 km long, with more than half located below sea level. It has been the most active of Kīlauea’s rift zones for at least the last ~200 years. The subaerial SWRZ extends ~35 km from the summit to the coast, and extends only a few kilometers offshore (Holcomb, 1987). The trend of the SWRZ changes by ~30° from southwest to south-southwest at the Pu‘ukou bend, which is situated about halfway between the summit of Kīlauea and the coast (Hazlett et al., 2019b).

The SWRZ is divided into two primary strands, the deeper seismic SWRZ and the shallower volcanic SWRZ (as defined by Holcomb, 1987; Poland et al., 2014) (Fig. 1). The seismic SWRZ extends as far as the Kamakai‘a Hills, and is marked mostly by earthquakes and seismic swarms related to magmatic intrusions. The volcanic SWRZ is delineated at the surface by an alignment of fissures, scoria cone alignments, faults, and ground cracks. The most prominent feature is the ~15 km-long Great Crack, which consists in a 5km-long, purely tectonic opening on its northern extent, and a ~10 km of eruptive fissure responsible for the 1823 CE eruption.

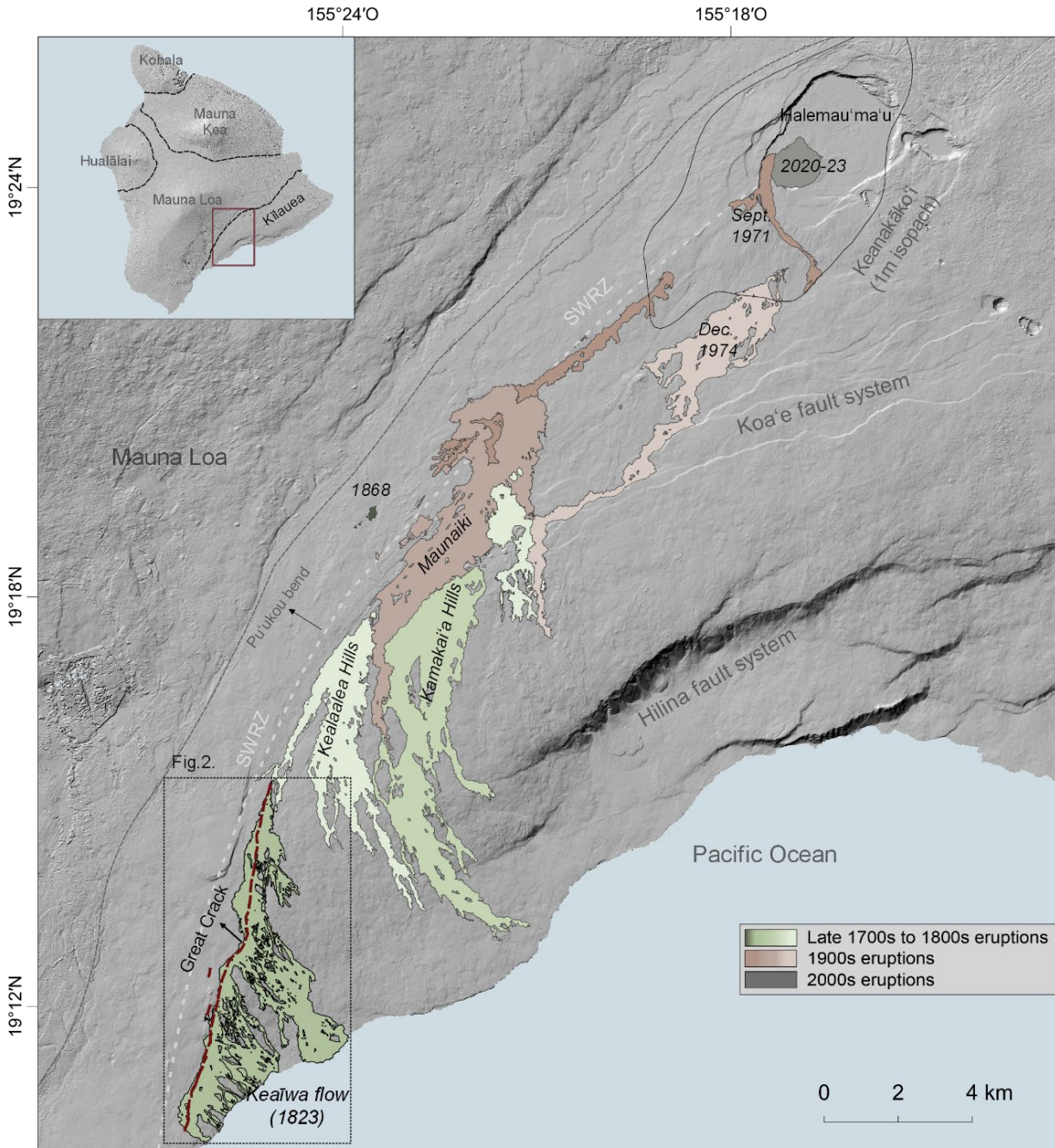


Fig. 1. Location of Kīlauea volcano (inset map) and lava flows within the Southwest Rift Zone that erupted from post-1790 CE to its most recent eruption in December 1974 (modified from Sherrod et al., 2021). For reference the recent eruptions (2020–23) within Halema‘uma‘u Crater are shown, as is the 1 m isopach of the ~1500 to early 1800s Keanakāko‘i Tephra (Swanson et al., 2014; Swanson and Houghton, 2019).

Southwest Rift Zone Eruptive Record

The historical record of eruptive activity within the SWRZ is generally proposed as beginning after the 1790 CE unit I explosive eruption of the Keanakāko‘i Tephra sourced from Halema‘uma‘u Crater (Swanson et al., 2014; Swanson and Houghton, 2019). The ~1500 to early 1800s Keanakāko‘i Tephra created an easily identifiable composite marker horizon within at least

15 km of Halema‘uma‘u Crater for dividing older (Observatory shield era) from younger historical lava flows (Swanson and Houghton, 2019) (Fig. 1), with unit I at 1790 CE being particularly easy to identify due to its accretionary lapilli-bearing nature. Hazlett et al. (2019) documented the stratigraphic position of the 1790 CE unit I tephra, confirmed via radiocarbon dating, in relationship to historical lavas within the middle SWRZ to demonstrate that eruptions occurred from the Kealaalea Hills and Kamakai‘a Hills after 1790 CE. The Kealaalea Hills lava flow is in turn covered in places by the 1823 CE lava flow, prompting Hazlett et al. (2019) to interpret both the Kealaalea Hills and Kamakai‘a Hills as erupting sometime between 1790 and 1823 CE (Fig.1). Eyewitness records and stories do not exist for these two eruptions; however, the 1823 CE lava flow was visited shortly after its eruption and was stated to still be hot to the touch, steaming, and incandescence was still visible within its source fissure (Ellis, 1827).

The SWRZ’s next eruption occurred ~45 years later, in 1868 (Coan, 1868), and subsequently erupted in 1919-1920 (Rowland and Munro, 1993), 1971 and 1974 (Holcomb, 1987; Neal and Lockwood, 2003; Sherrod et al., 2021). Since December 1974, the SWRZ has been volcanically quiet, although geophysical signals (i.e., seismicity, geodetics) indicate periods of magmatic unrest within the South Caldera and upper SWRZ regions.

1823 CE Eruption and Great Crack

The 1823 CE eruption occurred within the lower SWRZ in a part of Kīlauea called the Ka‘ū Desert due to its arid, sparsely vegetated surface. This eruption produced a sheet-like lava flow that covers an area of ~12.4 km², with ~6.4 km² of pāhoehoe-like proximal morphology, ~6 km² of slabby ‘a‘ā to ‘a‘ā (primarily present at >1 km away from the fissure vent), and ~0.01 km² of a phreatic debris field presumably from magma interacting with shallow groundwater near the coast (Fig. 2). Nowhere do the flows become well channelized, although proto-channels lacking levees appear in the transitional pāhoehoe-to-‘a‘ā dominated regions in satellite imagery.

This eruption has the distinction of being the first documented by an expedition of non-Hawaiian visitors. Based on eyewitness accounts from local inhabitants, Ellis (1827) reported:

‘The people of Kearakomo also told us that no longer than five moons ago Pele (Hawaiian goddess of volcanoes) had issued from a subterranean cavern, and overflowed the lowland of Kearaara (sic. Kealaalea) and the southern part of Kapapala. The inundation was sudden and violent, burnt one canoe, and carried four more into the sea. At Mahuku the deep torrent of lava bore into the sea a large rock, according to their own account near a hundred feet high, which, a short period before had been separated by an earthquake from the main pile in the neighborhood. It now stands, they say, in the sea, nearly a mile from shore, its bottom surrounded by lava, its summit rising considerable above the water.’

Ellis (1827) continues by stating of the lava:

‘It was highly scoriaceous, of a different kind from the ancient bed of which the whole valley was composed, being of a jet-black color and bright variegated lusters, brittle, and porous; while the ancient lava was of a gray or reddish colour, compact, and broken with difficulty.’

Stearns (1926) later provided detailed descriptions of this lava flow and its source fissure. He also noted that the mapped location of the 1823 CE lava flow, its source fissure, and in some cases source volcano changed significantly (see; Donn, 1901, Baldwin and Wright, 1907; Hitchcock,

1909, 1911) in the almost 100 years between the visit by Ellis (1827) before correcting the record with his own investigation (Stearns, 1926).

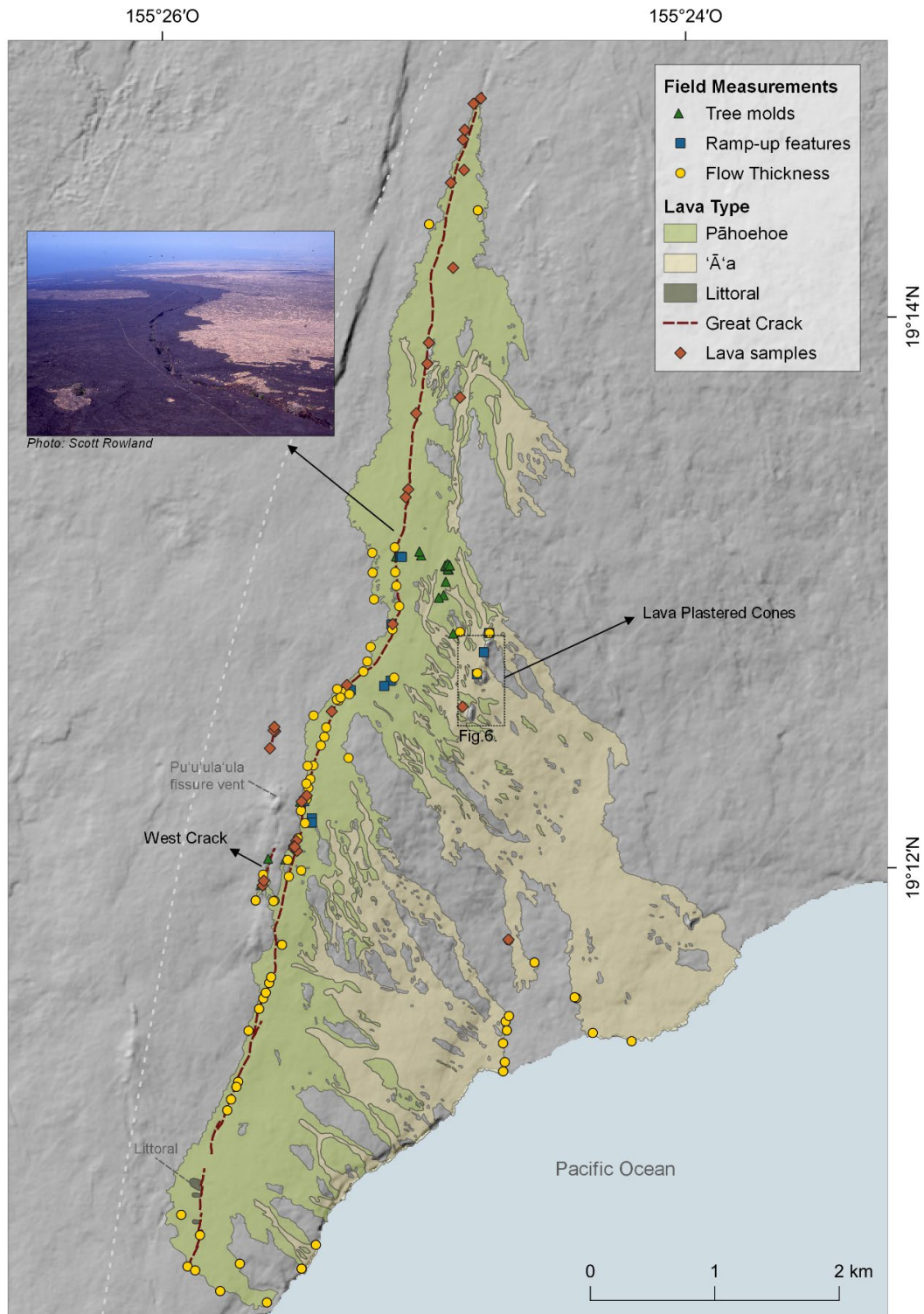


Fig. 2. Map showing the study area and an aerial view of a small portion of the fissure called the Great Crack. Included are the locations of field measurements and collected samples.

The 1823 CE lava flow erupted from a fissure that makes up 2/3 the Great Crack (originally referred to as the Ponahohoa by Ellis, 1827). The lava predominantly flowed to the southeast. The eruptive fissure part of the Great Crack is >10 m wide and >10 m deep for most of this length, and completely lacks constructional vent features (e.g., ramparts, scoria cones) (e.g., Stearns, 1926). The Great Crack extends a further 5 km uprift from the first appearance of the 1823 CE lava. However, this amagmatic segment is not as deep or wide as the 1823 CE magmatic portion. An additional, ~230 m-long fissure system occurs ~180–400 m west of the Great Crack, the West Crack (Fig.2). This fissure system consists of a set of four aligned (~200 m long), < 50 cm-thick lava flow pads along its northern extent, and a separate segment ~820 m to the south (~200 m long and aligned with the older Pu‘u‘ula‘ula fissure vent). The small lava flow erupted from the southern end of the west crack connects with the flows emitted from the Great Crack.

Numerous kīpuka are stranded across the 1823 CE lava flow, often displaying ramp-up features on their fissure-facing sides. This is an indication that the lava flow was moving fast enough to run up their slopes and, in some cases, overtop them entirely. The lava flow also mantles a line of scoria cones known as the Lava Plastered Cones, which are aligned roughly perpendicular to flow direction (Fig. 3A). The largest of the Lava Plastered Cones is completely covered by lava on its western side (the side facing the Great Crack) with the lava draping the outer and inner slopes of this scoria cone and showing some ponding in its interior (Fig. 3B). However, its eastern side (facing away from the Great Crack) shows no 1823 CE lava covering it.

Several small ballistic fields produced by phreatic explosions occur at the southern extent of the Great Crack (Stearns 1926). The ballistic fields are ~15–60 m in diameter with ejecta up to 60 cm in diameter. Stearns (1926) identified blocks being held tight by the underlying 1823 CE lava, which he interpreted as evidence that these phreatic blasts occurred before the lava had time to sufficiently cool and solidify (i.e., within hours or less of the lava erupting).

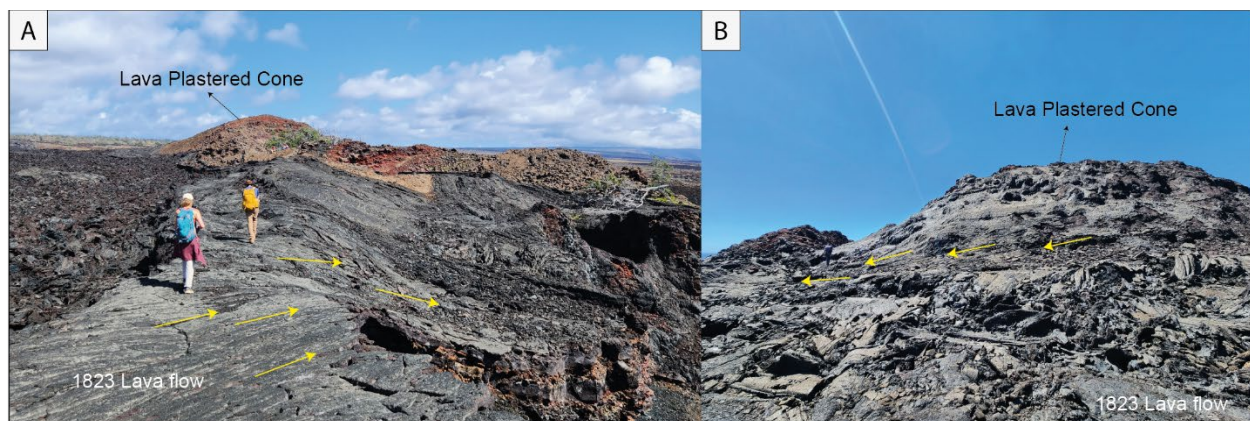


Fig. 3. Lava Plastered Cones. A) The photo shows the northernmost Lava plastered cones surrounded by the 1823 lava flow, yellow arrows show the direction of the flow perpendicular to the cones alignment, and B) shows the tallest cone covered by the 1823 lava flow.

Methods

Fieldwork and Sample Collection

To better characterize the features along the eruptive fissure part of the Great Crack and 1823 CE lava flow, we conducted detailed fieldwork and collected 48 samples for petrography and whole-rock, glass, and olivine chemistry. We documented morphological features to help

understand the emplacement of the 1823 CE lava flow and its relationship to the Great Crack. Lava flow features documented and measured include near-vent lava flow surface morphology, fissure drain-back features, tree molds, lava balls, and sporadic spatter from sloshing of lava against the fissure walls. We measured thicknesses of proximal and distal lava flow margins, tree molds (pre- and post-draining), lava flows around kīpuka margins and along the length of the Great Crack (Fig. 2). We also measured the run-up heights and angles of ramp-up features (e.g., tumuli, Lava Plastered Cones, ramparts). Additionally, while the year of eruption of the 1823 CE lava flow is not in question, four charcoal samples were analyzed to place it within the context of previously analyzed charcoal samples from other SWRZ eruptions that occurred in the early 1800s. Field, chemical, and petrographic data all provide key inputs for understanding and modeling the rheological behavior of the 1823 CE lava flow, as detailed below.

Chemistry

Wavelength Dispersive X-Ray Fluorescence (WD-XRF) Spectrometry

A total of 26 samples were analyzed for major-oxide and trace-element chemistry by wavelength dispersive X-ray fluorescence (WD-XRF) spectrometry. Samples consist of near-fissure glassy spatter (n = 10), the surface of the pāhoehoe-like sheet flow (n = 11), transitional pāhoehoe to ‘a‘ā flow surface crust and clinker (n = 2), and the highly vesicular and glassy juvenile interiors of lava balls (n = 3). A single sample (K21-DD56_R) was run twice as a duplicate analysis to check for internal precision and accuracy.

Samples were ultrasonicated in distilled water for an hour to remove adhering sulfur species, and ~25 g of material was sent to the Hamilton Analytical Laboratory at Hamilton College in Clinton, New York, USA for analyses (using the methods of Johnson et al., 1999). Fresh rock chips were powdered in an Al-swing mill, diluted with a flux of di-lithium tetraborate ($\text{Li}_2\text{B}_4\text{O}_7$) at a 2:1 ratio (flux to rock), and fused to a bead at 1000°C. The bead was powdered, refused, polished to provide a smooth surface, and analyzed on a Thermo ARL Perform’X spectrometer for 10 major-oxides and 30 trace-elements. Loss on ignition (LOI) is measured for all samples by heating overnight in silica crucibles at 900°C. Each run included analysis of BHVO-1 standards, for which accepted values can be found in Jochum et al. 2016. All WD-XRF analyses are reported as 100% anhydrous with original analytical loss on ignition (LOI) and totals given.

Electron Probe Microanalysis (EPMA)

Glass and mineral (i.e, olivine) chemical analyses were performed on 11 samples of glassy spatter using the JEOL 8500F Field Emission Gun Hyperprobe at the University of Hawai‘i at Mānoa, Honolulu, USA using the Probe for EPMA software (Donovan and Tingle, 1996). Spot analyses of glasses were performed using an accelerating voltage of 15 keV, a 10 nA beam current, a 6–10 μm beam diameter, and count times of 20 s (Si, Ti, Na, K, P), 30 s (Fe, Mn), and 70 s (Al, Mg, Ca, Cl). Eight spot analyses were acquired for each glass sample, with glass standards analyzed repeatedly to monitor for analytical drift. The accuracy of the method is less than 0.5% for SiO_2 , Al_2O_3 and P_2O_5 , less than 1% for FeO and MgO and greater than 1% for TiO_2 , MnO, CaO, Na₂O and K_2O . The precision is less than 1% for SiO_2 , Al_2O_3 , FeO, MgO and CaO, less than 5% for TiO_2 and Na₂O and greater than 5% for MnO, P_2O_5 and K_2O .

Olivine spot analyses were done using a 20 keV accelerating voltage and a 200 nA beam current with a diameter of 10 μm. Count times were 40s (Si, Na, Ni), 30 s (Fe, Mn), 50 s (Ti, Ca, K, Cr), and 56 s (Al, Mg). Core and rim regions were analyzed to check for possible zoning.

Standards used for glass and olivine calibrations include Verma Garnet (Mn), San Carlos and Springwater olivine (Si, Fe, Mg), Sphene glass (Ti), Lake County plagioclase (Ca), synthetic olivine from CalTech (Ni, Ca, Mn), Durango apatite (P), and two glasses were used as check standards (A-99, VG-2). The accuracy of the methods is less than 1% for SiO₂ and MgO, less than 5% for FeO and MnO and greater than 5% for Cr₂O₃. The precision is less than 1% for SiO₂, FeO and MgO, less than 5% for MnO and greater than 5% for Cr₂O₃.

Radiocarbon Dating

Four samples of charcoal were analyzed by accelerator mass spectrometry (AMS) at DirectAMS in Bothell, Washington, USA. These samples underwent pre-treatment and were analyzed on a National Electrostatics Corporation (NEC) 1.5 SDH Compact Pelletron Accelerator Mass Spectrometer (Tate et al., 2023).

Modeling

Lava flow modeling was conducted using the VolcFlow computer software (Kelfoun and Druitt, 2005; Kelfoun and Vallejo Vargas, 2015). VolcFlow has been widely used to model rheology, dynamics, deformation, and emplacement of different volcanic products and processes, including lava flows, dense and dilute pyroclastic flows, debris avalanches, and tsunamis (Charbonnier et al., 2013; Gueugneau et al., 2021; Kelfoun, 2021; Kelfoun and Vallejo Vargas, 2015; Marquez et al., 2022). VolcFlow is a depth averaged model that uses an x and y coordinate system parallel to a topographic surface to simulate various rheologies (e.g., plastic, viscous, Coulomb, etc.) (Kelfoun and Druitt, 2005; Kelfoun and Vallejo Vargas, 2015). The mathematical model incorporates shallow-water equations (SWEs), assuming that flow is shallow compared to horizontal distance (Kelfoun and Druitt, 2005; Cordonnier et al., 2015; Hager et al., 2019).

Other models such as FLOWGO were initially considered to solve for potential lava flow emplacement velocities, because it incorporates downflow cooling and the ensuing rheological changes (Harris and Rowland, 2001, 2015). However, that code is designed for channelized, cooling-limited flows. As argued further below, the flow was likely volume- rather than cooling-limited and never developed well-formed channels. In addition, downflow cooling of the 1823 CE lava flow has been inferred to be relatively small (Soule et al., 2003). For these reasons we opted to use VolcFlow.

To model 1823 CE eruption, VolcFlow uses topography, volume, time, yield strength, viscosity and density to simulate the direction, velocity and momentum of the lava flow. The momentum is amount of mass that is moving at a certain velocity. In this case, we used the current topography, after 1823 eruption, due to the short and constant thickness it has. The Keaīwa lava flow mantles very well the pre-existing topography, and was emplaced in a single pulse.

Results

Field Observations and Measurements

We measured lava flow thicknesses throughout the extent of the 1823 CE flow field. Thicknesses range from 15 to 110 cm along the margins of the flow, 13 to 64 cm along the length of the Great Crack, and up to 312 cm (pre-draining) and 160 cm (post-draining) for tree molds within the interior of the flow field (Fig. 4). These thicknesses illustrate how unusually thin the 1823 CE lava flow is over its entire ~12.4 km² extent. By comparison, pāhoehoe and ‘a‘ā lava

flows from Kīlauea typically achieve thicknesses of tens of meters (e.g., Katz and Cashman, 2003; Harris and Rowland, 2015; Neal, 2019). This does not account for lava that flowed into the ocean, nor any potential underwater vents that may have formed if the dike intrusion extended into the submarine realm. Finch (1940) noted that the 1823 CE eruption likely corresponds with $\sim 500 \times 10^6 \text{ m}^3$ of summit caldera subsidence at Halema'ūma'ū, although this estimate is much larger than the $10 \times 10^6 \text{ m}^3$ erupted volume that he noted for the 1823 CE flow field.

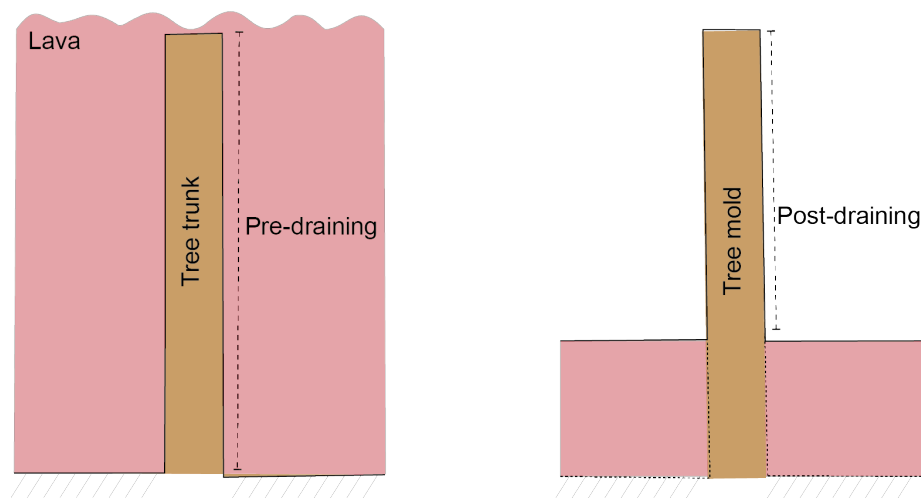


Fig. 4. The sketch shows the criteria used to measure tree molds.

Near-vent features and field relations

Field observations helped in documenting volcanic features, such as lava drain-back, ramp-up features, lava balls, and glassy, air-quenched spatter situated proximal to the Great Crack (within $\sim 50 \text{ m}$) (Fig.5). Furthermore, extensive sections of the walls of the Great Crack are coated by thin drain-backs of the lava into the fissure system. The 1823 CE lava consistently covers the walls of the Great Crack fissure system along most of its length. Lava balls also occur along much of the length of the fissure part of the Great Crack. These lava balls generally consist of older, ripped-up wall rock coated in 1823 CE lava, as well as highly vesicular, juvenile glassy 1823 CE lava that is coated in a shell of denser 1823 CE lava. The lava balls are mostly exposed within the walls and along the top of the Great Crack, but some have been ejected up to 5 m away from the fissure. Additionally, sparse and localized juvenile glassy spatter (1-5 cm thick) occurs along the fissure part of the Great Crack, having been ejected as much as 50 m away. This fluidal spatter was too sparse to build any constructional vent features.

Ramp-up structures have been documented around the entire area covered by the 1823 CE lava flow, but most of them are in the northeastern part of the 1823 CE flow field. These structures can be used to estimate the velocity of the flow front (e.g., Baloga et al., 1995; Guest et al., 1995). Previous reports state that the Lava Plastered Cones stand up to $\sim 10.5 \text{ m}$ tall from the flow top (Stearns, 1926; Guest et al., 1995). Our field measurements and digital elevation models confirm this, show an angle between $26\text{--}28^\circ$, and a flow thickness of $\sim 11 \text{ cm}$ at the top of the Lava Plastered Cones. We measured ramp-up features on previously emplaced tumuli and scoria cones, which yield run-up heights of 4–10 m at angles of $30\text{--}50^\circ$. The slope of much of the rest of the topography that encompasses the 1823 CE lava flow is generally $<5^\circ$, although it is steeper closer to the coastline.

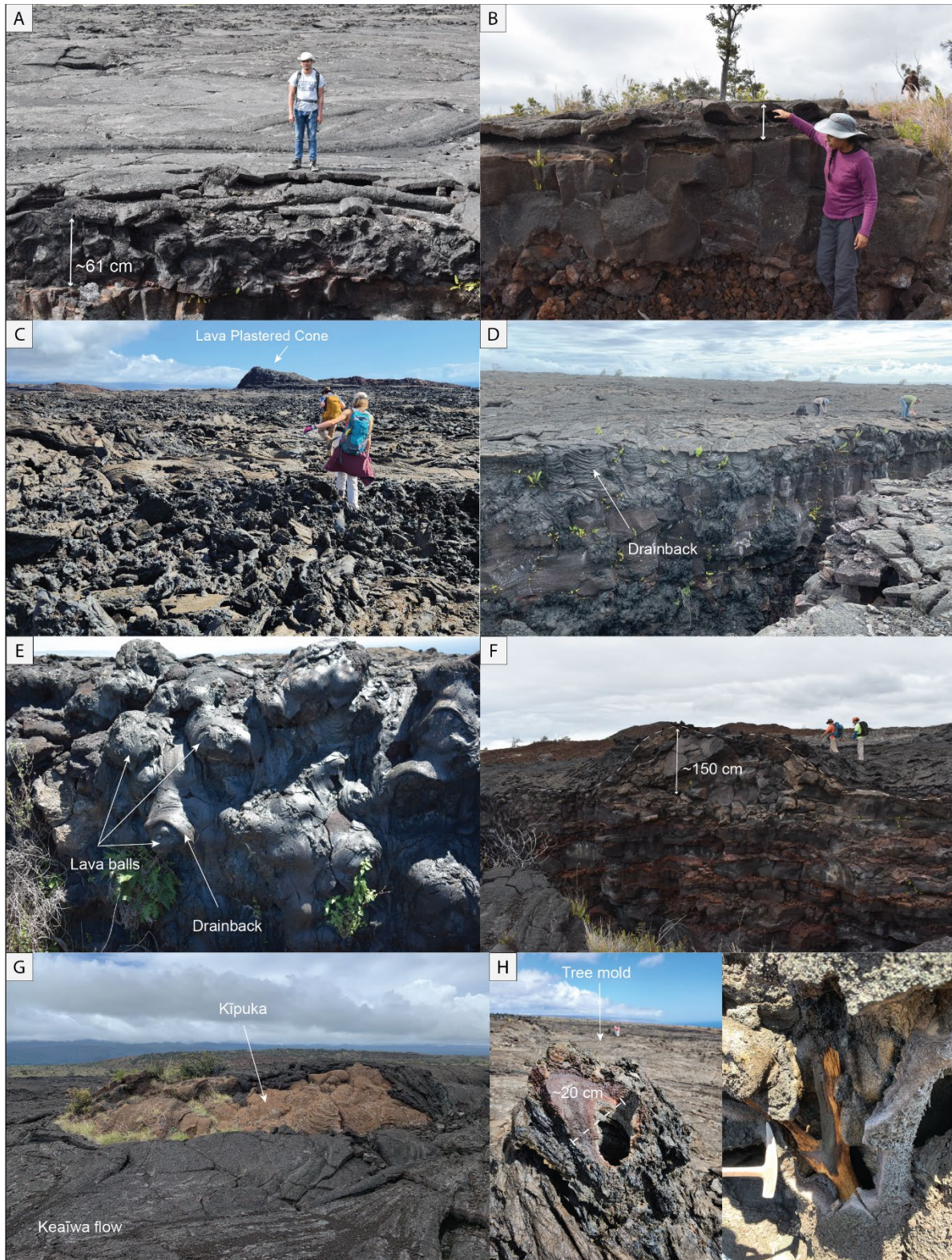


Fig. 5. Photos showing volcanic features that interacted with the 1823 CE lava flow. A) pāhoehoe-like sheet flow, B) 1823 lava flow thickness at the inner wall of the Great Crack, C) transitional lavas that cover a transitional area between A and B, D) lava drain-back features that cover lava balls and the fissure part of the Great Crack, E) sequences of lava balls along the fissure wall, F) ramp-up of 1823 CE lava that covers a pre-existing tumuli, G) Kīpuka of older lava that has been partially overrun and surrounded by the 1823 CE lava flow, and H) tree molds with charred wood and one that is hollow.

Petrographic Characteristics

Lava from juvenile, glassy spatter and flows of the 1823 CE eruption are generally crystal-poor (< 5%). Phenocrysts and microphenocrysts consist in olivine, clinopyroxene, and plagioclase. Millimetric gabbroic crystal clots (plagioclase + pyroxene ± olivine) are commonly found in 1823CE samples but not in samples from the preceding eruption (Kealaalea Hills). The lava flows that originated from the west crack are richer in crystals than those that originated from the Great Crack.

Chemistry

Whole-Rock Chemistry

Major-oxide and trace-element abundances from the 1823 CE lava overlap with other tholeiitic basalt compositions erupted from Kīlauea (e.g., Easton and Garcia, 1980; Wolfe and Morris, 1996; Pietruszka and Garcia, 1999; Garcia et al., 2000, 2003, 2021; Thornber et al., 2015; Gansecki et al., 2019; Pietruszka et al., 2021). Samples from the west crack are slightly more mafic with MgO at 7.86 ± 0.05 wt. % (average ± standard deviation) compared to the 7.44 ± 0.07 wt. % MgO analyzed from Great Crack erupted samples. Incompatible elements also show a slightly difference between both sites. Samples from the west crack contain 2.45 ± 0.01 wt. % TiO₂, 0.46 ± 0.004 wt. % K₂O, and 11 ± 0.05 wt. % CaO, slightly lower than Great Crack samples that contain 2.51 ± 0.01 wt. % TiO₂, 0.45 ± 0.005 wt. % K₂O, and 11.15 ± 0.07 wt. % CaO (Fig. 8).

Glass Chemistry

Glass chemistry was only performed on juvenile, glassy, air-quenched spatter samples collected only the length of the Great Crack. These were used as they are the most rapidly quenched lavas from the 1823 CE lava flow, and therefore their glass compositions are the least affected by microlite growth during slow cooling. Our glass analyses yield MgO abundances of 6.40 ± 0.10 wt. % which are less mafic than Kealaalea Hills lavas (6.80 ± 0.04 wt. % MgO), Halema‘uma‘u 1832 eruption (7.55 ± 0.10 wt. % MgO), and Halema‘uma‘u 1877 eruption (6.79 ± 0.05 wt. % MgO), and Great Crack MgO is more mafic than Unit L4 from Keanakāko‘i tephra which has 5.91 ± 1.60 wt. %.

MgO abundances were used to calculate eruption temperatures of $1,153 \pm 13^\circ\text{C}$ (using the MgO-in-glass thermometer of Shea et al., 2022). These temperatures are similar to the $\sim 1,150^\circ\text{C}$ for the 1823 CE lava flow that were calculated by Soule et al. (2003). Additionally, Soule et al. (2004) calculated a temperature decrease of $6 \pm 1^\circ\text{C}/\text{km}$ away from the Great Crack, although these temperatures vary more based on their lava flow morphologies with an important temperature boundary being $1,140 \pm 1^\circ\text{C}$ between pāhoehoe and ‘a‘ā morphologies. In all cases, our glass analyses confirm that the 1823 CE lava flow was a typical tholeiitic basalt with a common eruption temperature for Kīlauea.

Olivine Chemistry

Olivine compositions range between Fo_{75.6} and Fo_{83.8} (n = 78) in cores and rims. Olivine core compositions from the 1823CE eruption are in the range Fo_{76.1–83.8}, with a peak at Fo_{78.5}. Rim compositions range from Fo_{75.6–81.6} with a peak at Fo_{78.3}.

To understand the spatial and temporal context of the 1823 CE eruption, we compare its olivine phenocrysts to that of other SWRZ and Halema‘uma‘u Crater olivine from the Keanakāko‘i Tephra period and the early 1800s (Fig. 6 and 7). Olivine core compositions from Kealaalea Hills eruption (erupted sometime between 1790–1808 CE; Downs et al., 2023) from the SWRZ have slightly

higher Fo contents overall, with a range $Fo_{77.2-85.4}$, and a peak at $Fo_{82.3}$. Rim compositions are also slightly higher than in 1823 CE lavas ($Fo_{76.3-84.7}$ with a peak at $Fo_{80.5}$). Both 1823CE and Kealaalea olivine compositions show much lower Fo than summit lavas from the same period. Olivine core compositions from the Halema'uma'u Crater in 1832 CE have $Fo_{87.7-90.0}$ with a peak at $Fo_{89.1}$, and rim compositions of $Fo_{82.2-87.7}$ with a peak at $Fo_{84.3}$. Olivine core compositions from Keanakāko'i Tephra unit L4 (erupted in the early 1800s CE from Halema'uma'u Crater) have $Fo_{84.8-88.7}$ with a peak at $Fo_{86.6}$, and rim compositions of $Fo_{79.3-87.0}$ with a peak at $Fo_{84.1}$.

In general, summit eruptions during the Keanakāko'i Tephra explosive period from ~1500 to the early 1800s CE are dominated by high-Fo olivine (Fo_{80-90} , see Lynn and Swanson, 2022). Lynn and Swanson (2022) propose that there is a clear difference in olivine core and glass compositions after periods of caldera collapse or small-scale crater collapse at Kīlauea. Ellis (1827) states that the lava lake at the summit in Halema'uma'u Crater had drained by >100 m not long before his arrival at the summit, based on the appearance of a glassy, black ledge to the summit lake may have drained in conjunction, or in response, to the 1823 CE eruption. However, the Fo contents of 1823 CE olivine phenocrysts cores are lower than those typical of fresh, summit-derived magmas. Despite that, temperature obtained from glass analysis for the 1823 CE eruption lies on the typical range of temperature for basaltic lavas at Kīlauea, so does its viscosity.

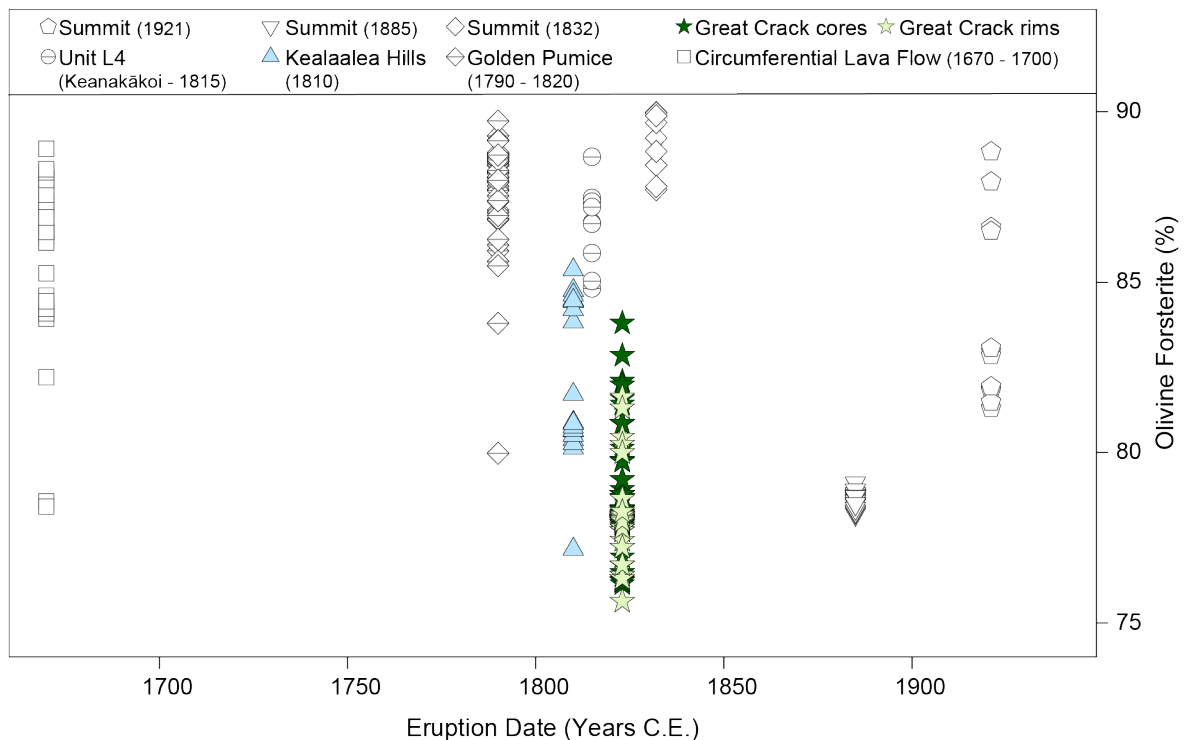


Fig. 6. Comparison of the Forsterite percentage of the Keaīwa lava flow and Keala'alea hills compared with other Kīlauea eruptions that occurred around the same period of time at the summit and SWRZ. The symbols are larger than the analytical errors for the data (Fo from the Great Crack). Chemical data shown for comparison are from Garcia et al. (2003), Lynn et al. (2017), Lynn and Swanson (2022) and Downs et al. (2023).

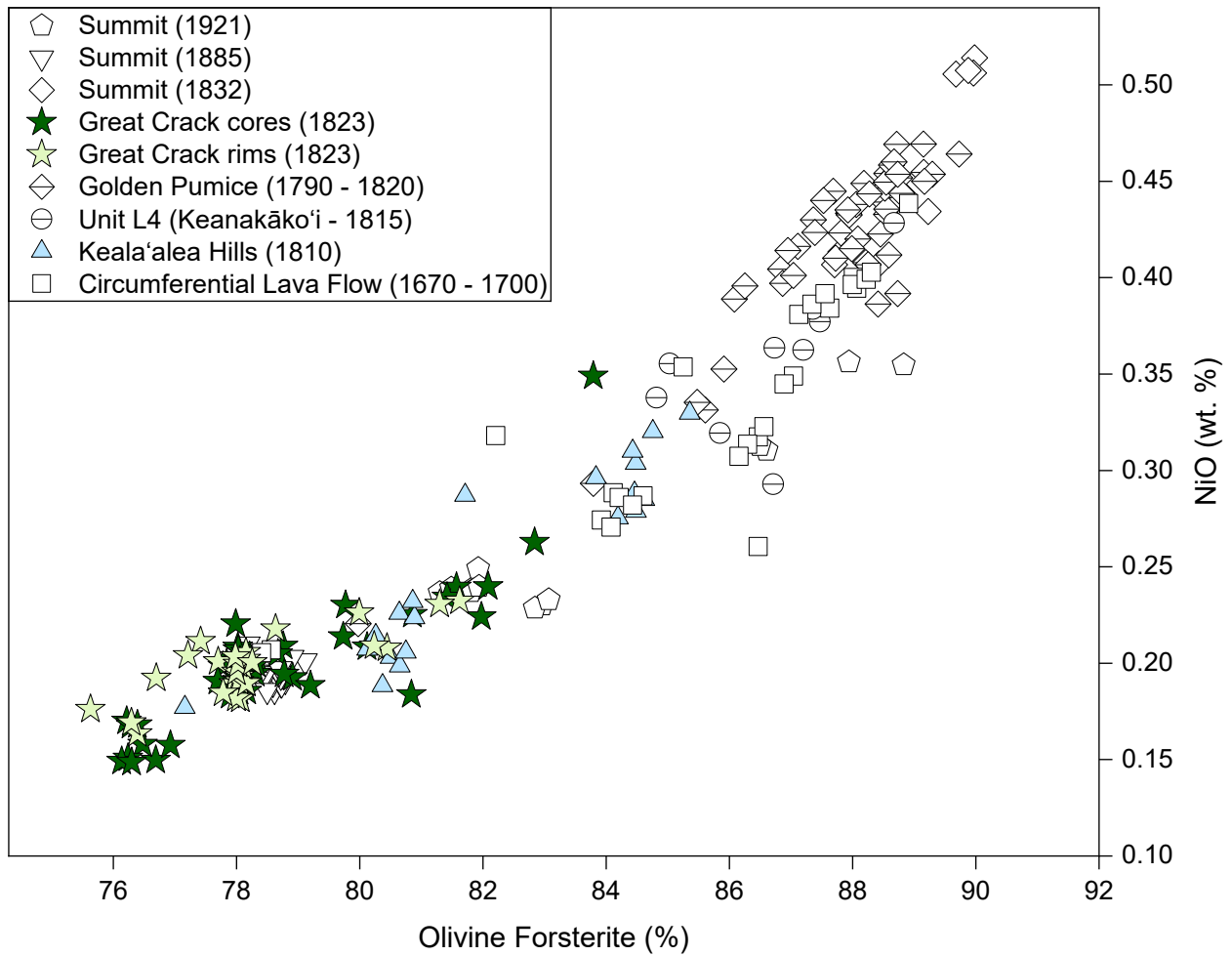


Fig. 7. Plot shows a comparison of Olivine Forsterite vs NiO among other eruption of Kīlauea that occurred during the same period of time. The symbols are larger than the analytical errors for the data (Fo from the Great Crack). Chemical data shown for comparison are from Garcia et al. (2003), Lynn et al. (2017), Lynn and Swanson (2022) and Downs et al. (2023).

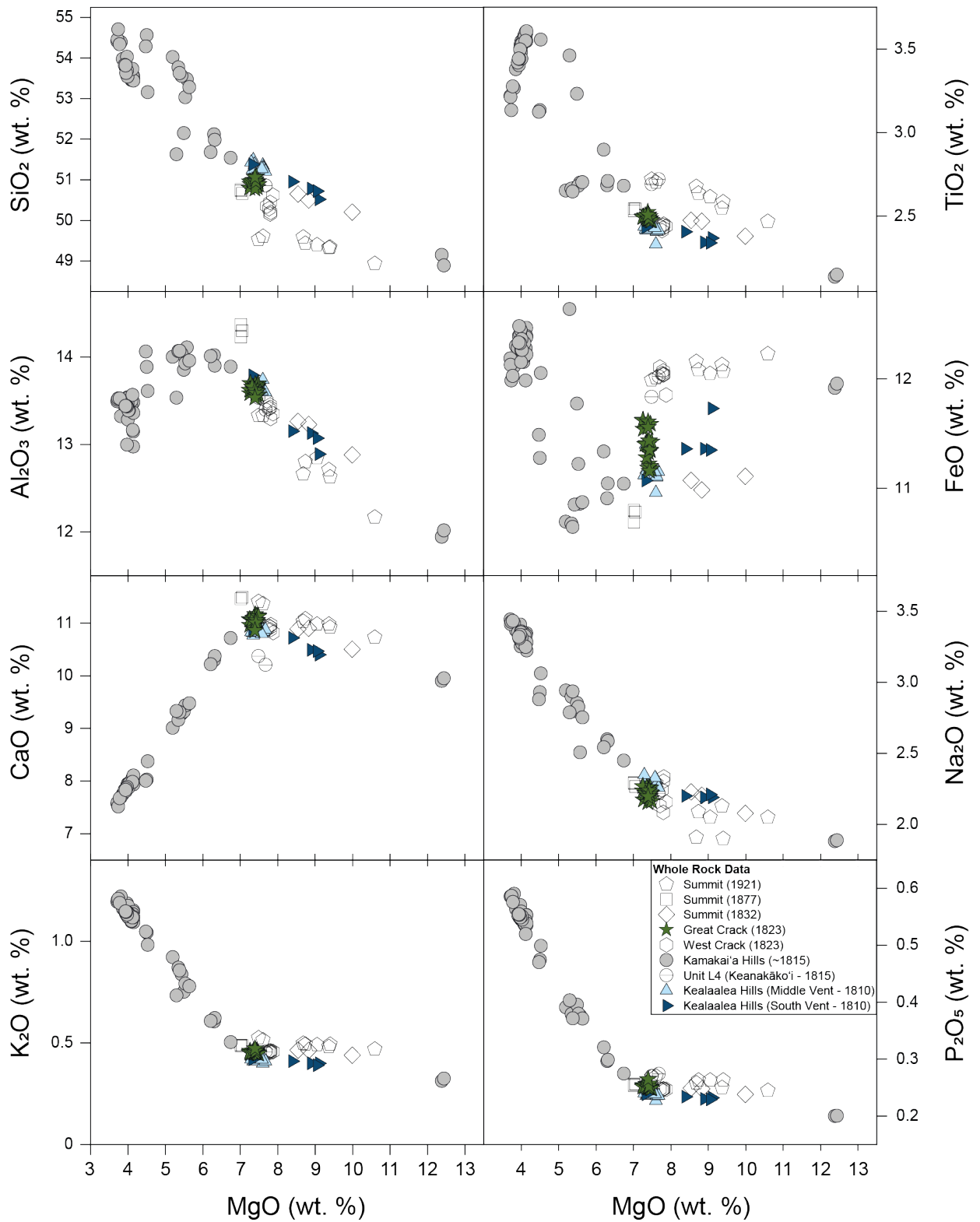


Fig. 8. The plots show the results of bulk rock analyses from the Keaīwa lava flow and Keala'alea hills compared with other Kīlauea eruptions that occurred around the same period of time at the summit and SWRZ. The symbols are larger than the analytical errors for the data. Chemical data shown for comparison are from Garcia et al. (2003), Lynn et al. (2017), Lynn and Swanson (2022) and Downs et al. (2023).

VolcFlow Modeling

Effusion rates and flow front velocities

We ran approximately 250 models to calculate the minimum effusion rate and velocity necessary for a lava flow originating from the Great Crack to overtop the Lava Plastered Cones (~10 m) and ramparts within the southwestern region of the 1823 CE lava flow. Yield strength and viscosity are key inputs to the model, and are approximated as being constant for the duration of the flow. We justify this approximation by noting that lava flow thickness at the margins varies little along the Great Crack and from proximal to distal regions. A melt viscosity of ~140 Pa/s was calculated using the model of Giordano et al. (2008) with glass compositions measured by EPMA and a maximum temperature of $1153 \pm 13^\circ\text{C}$ calculated using the MgO-in-glass thermometer of Shea et al. (2022). A bulk viscosity of up to 250 Pa/s was then obtained from the equations by Phan-Thien and Pham (1997) using a crystallinity of 5 vol.%, a vesicularity of 40 vol.%, and assuming bubbles and phenocrysts have roughly the same size. Given that our modeling objective is to explore the lower bounds of effusion rates and velocities required for the 1823 CE lava flow to overtop pre-existing cones and ramparts, we tested a bulk viscosity range of 100–200 Pa/s in the models. Testing higher values of viscosity would only lead to requiring higher effusion rates and velocities to overcome the same topographic barriers. The retarding stress component for lava flows is yield strength and controls the final thickness of the modeled flows. We adopted a yield strength (τ_y) of 500 Pa, which resulted in a final flow thickness comparable to those that we measured in the field (Fig. 9). Additionally, due to the importance of the resolution of the digital elevation model (DEM) when testing the accuracy of any terrain-dependent model, we first used the USGS 1 m-resolution lidar DEM, which was not feasible in terms of simulation time. Thus, we reduced its resolution to 2 m, which provided reasonable simulation times (ranging from a few minutes up to 1 hour per run depending on the model parameters used).

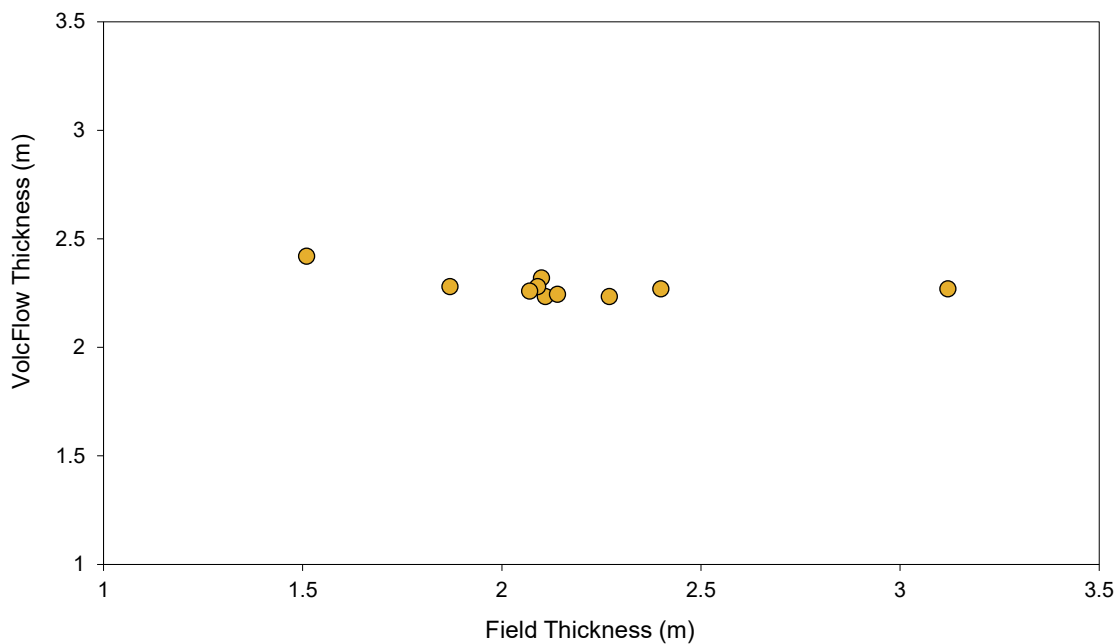


Fig. 9. Comparison between thicknesses obtained from VolcFlow and thicknesses measured in the field.

We tested a parameter grid of volume and eruption duration in the code while keeping them in the range of the total erupted lava field ($12 \times 10^6 \text{ m}^3$) (Stearns, 1926). We ran models for volumes between 3×10^6 to $12 \times 10^6 \text{ m}^3$, and durations from 100 to 2,000 s, which cover a wide range of effusion rates (5×10^3 to $18 \times 10^3 \text{ m}^3/\text{s}$) along the length of the fissure (Fig. 10). However, we focused the simulations on accurately replicating the coverage of the 1823 CE lava flow over the highest structures in the flow field, the Lava Plastered Cones.

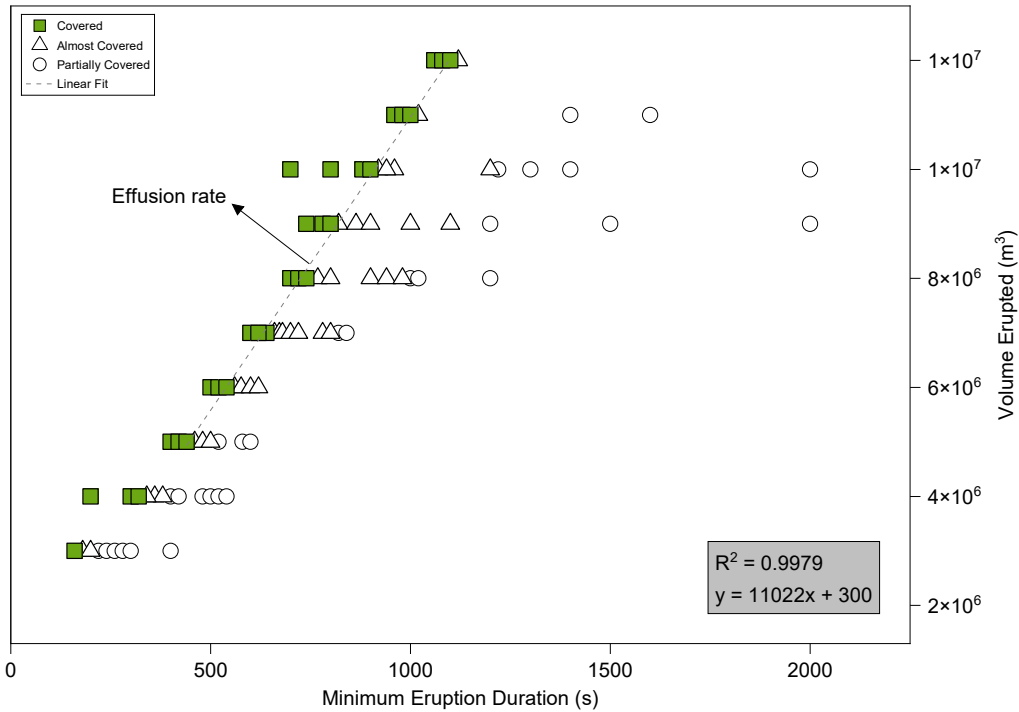


Fig. 10. Results from lava flow modeling. Linear relationship between time vs volume show the minimum effusion rate (boundary between the squares and the triangles) required for the lava flow to cover the Lava Plastered Cones.

Three main model outputs were examined: a video of the simulation showing the fraction of the Lava Plastered Cones covered by the 1823 CE lava flow, as well as two plots of velocity (maximum velocity across the flow field, V_{max} , and local flow velocity just north of the largest of the Lava Plastered Cone, V_{cone}). Simulation results were marked as successful when the lava flow completely covered the area of the Lava Plastered Cones as shown in the orthophoto and verified in the field (Fig. 11). Conversely, a lava flow that did not overcome the Lava Plastered Cones or left patches uncovered were marked as unsuccessful. The models that provided very narrow or small uncovered patches were assigned as almost complete and were used to mark the limit of effusion rate needed for the lava flow to overtop the Lava Plastered Cones.

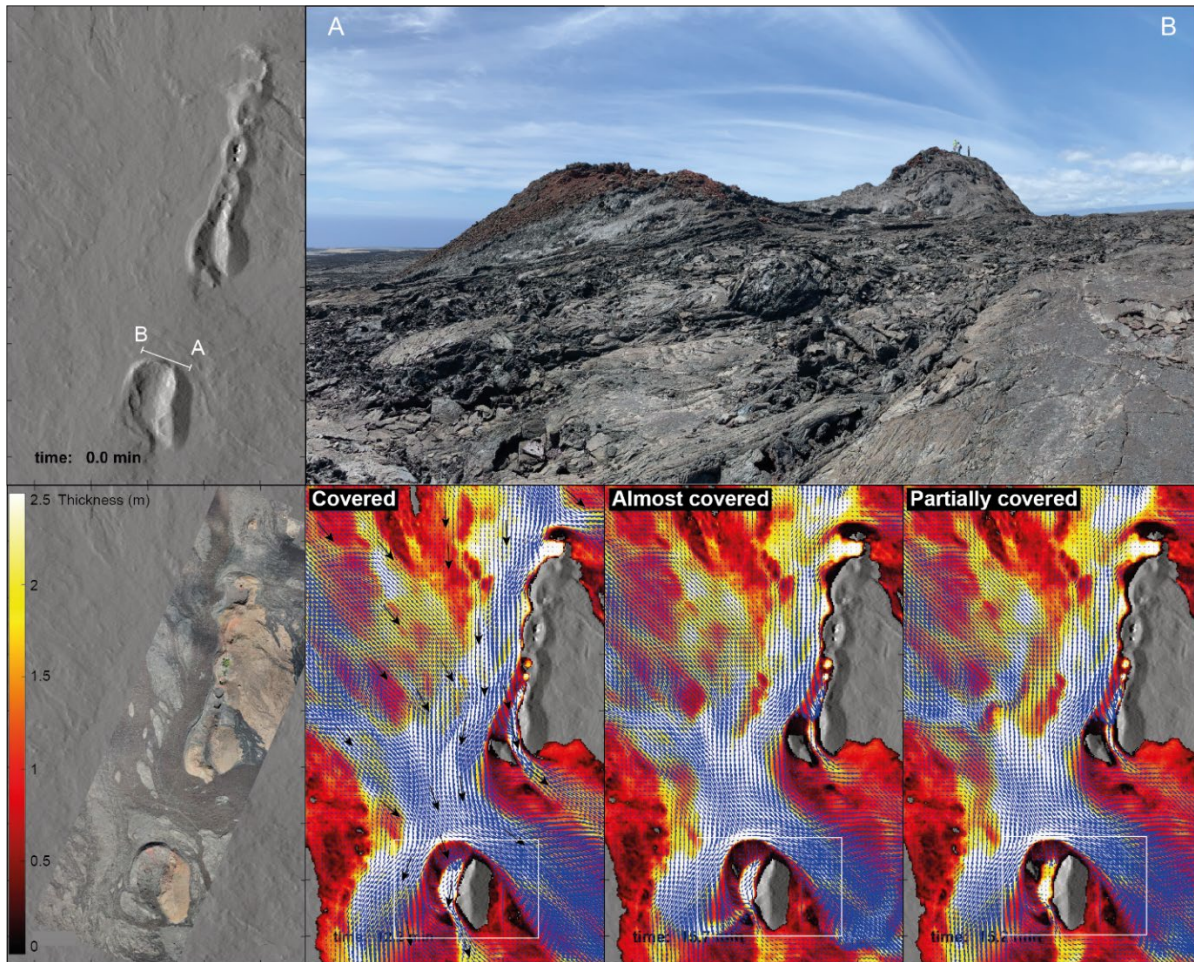


Fig. 11. Lava Plastered Cones in VolcFlow. The 2 m DEM's show the criteria used to classify the models. White squares show the area used to classified whether the flow is succesful or not. Black arrows show flow direction.

The minimum bulk effusion rate needed for the 1823 CE lava flow to completely overcome the highest (~10 m) of the Lava Plastered Cones is 10,000–11,000 m³/s for volumes of $>4 \times 10^6$ m³ with a velocity of 11 m/s (Fig. 12 and 13). Assuming a vesicularity of 40 vol. %, dense rock equivalent effusion rates are 6400–6800 m³/s. Guest et al. (1995) calculated velocities of 12–15 m/s assuming a lava flow thickness that was 2 m thicker than the evidence of tree molds they had at that time. Our model results in a maximum thickness between 2 and 2.5 m total, similar to the average thickness measured at tree molds in the interior of the flow. Our models can replicate near perfectly the 1823 CE actual flow field and its momentum around the Lava Plastered Cones which provides confidence about the accuracy of the simulations and our assumption of the eruption mechanism (Fig.14).

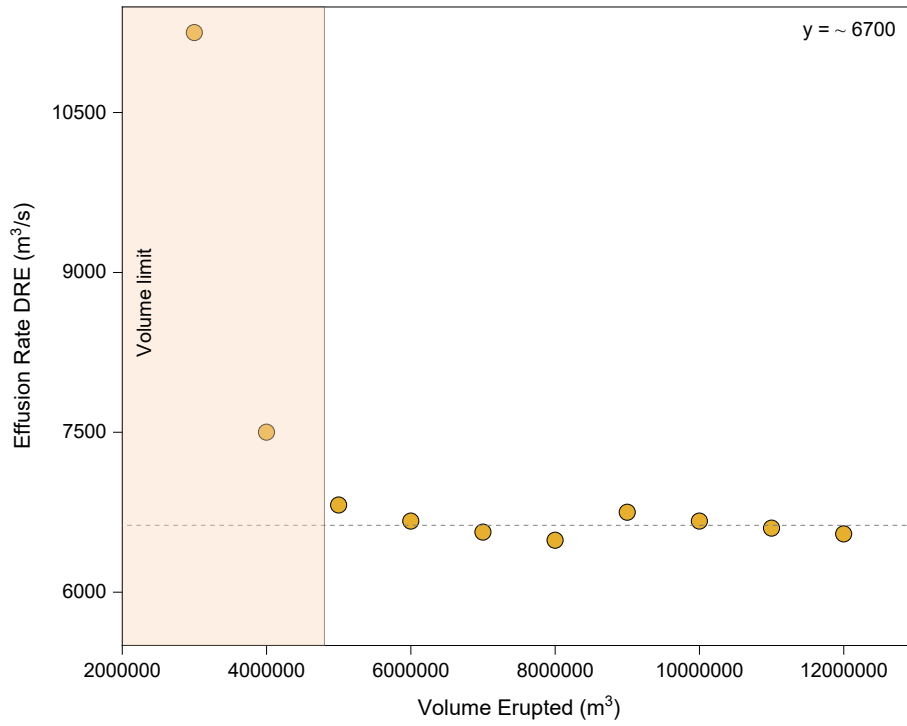


Fig. 12. Effusion rate required to cover a flow field area. Effusion rates behave consistent for volumes $\geq 5\,000\,000\text{ m}^3$.

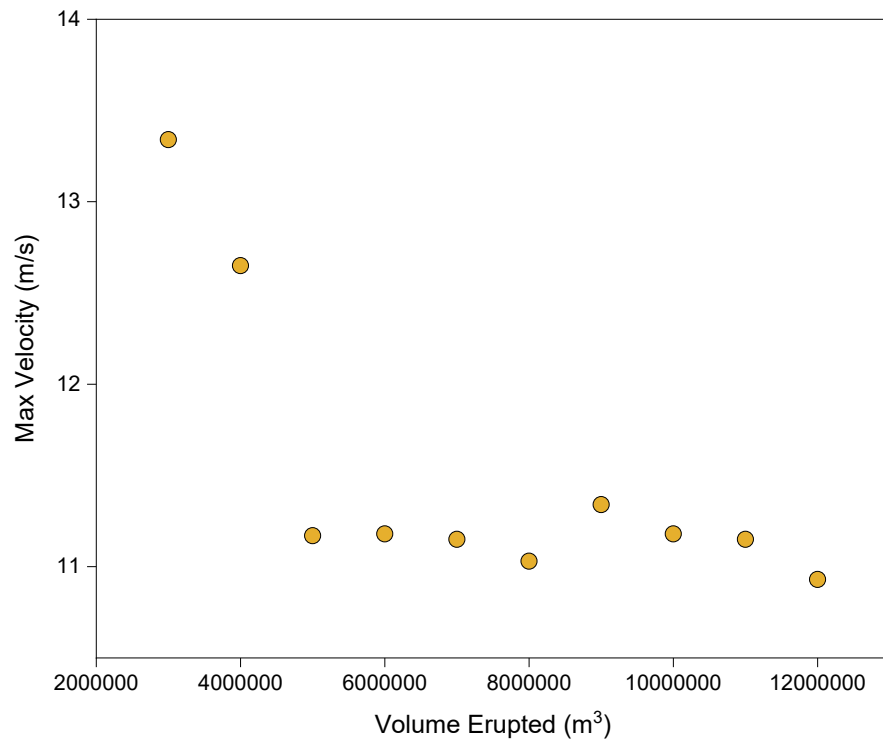


Fig. 13. Maximum velocity reached when the lava flow reaches the Lava Plastered Cones.

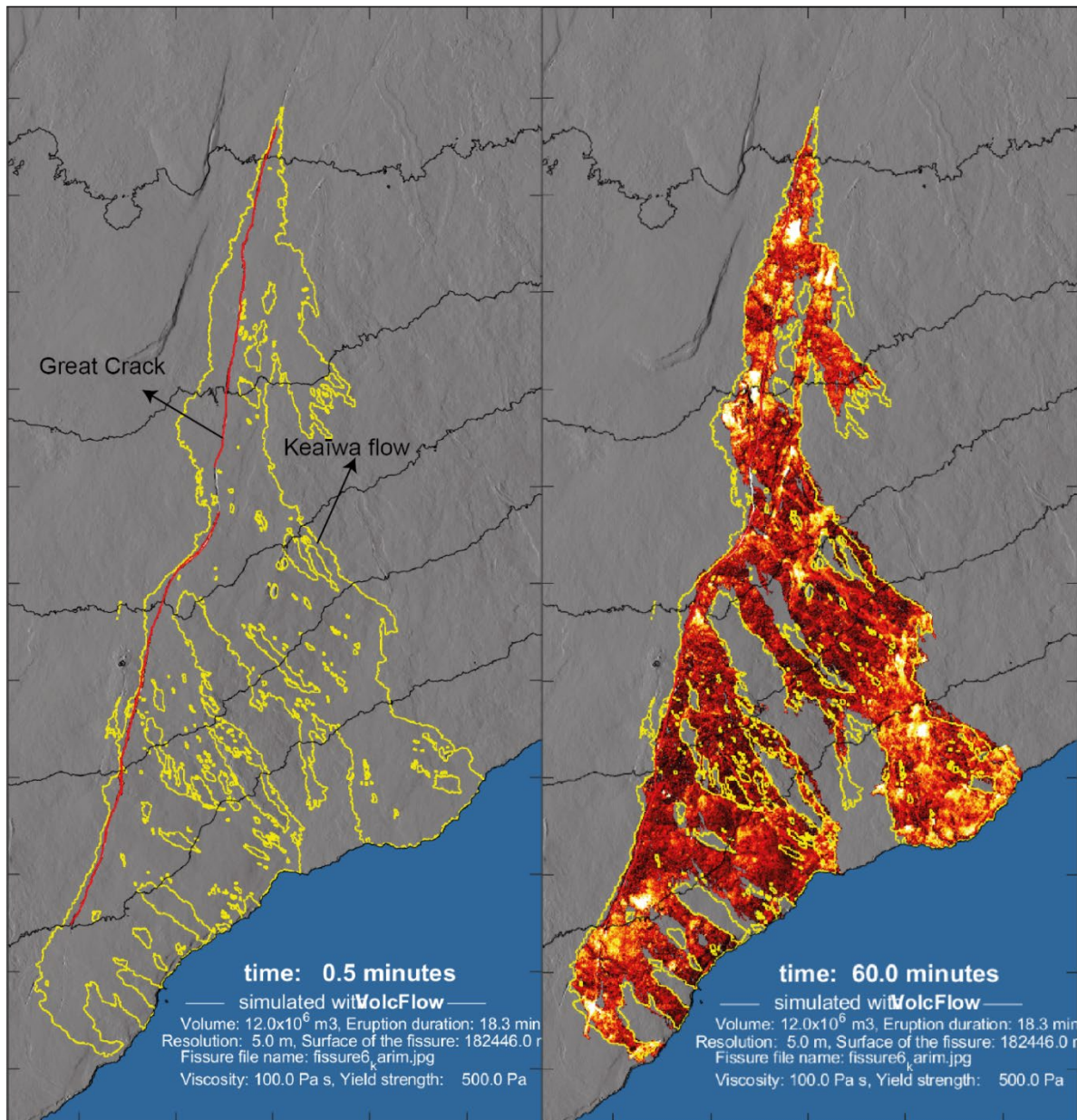


Fig. 14. The complete extent of the VolcFlow simulation for the 1823 CE eruption. It shows a good fit of the simulation within the actual flow field outline. Black lines are topographic contour lines.

Comparisons to eruptions worldwide show that high eruption rates can occur (Fig. 15). Eruptions with high effusion rates occurred at Kīlauea during Mauna Ulu eruption in 1969, and Pu‘u‘ō‘ō in 1984 and 1985 (Lipman & Banks, 1987; Rowland & Walker, 1990; Dietterich et al., 2021). However, these eruptions occurred during a longer period of time, and their lava flows did not go too far from the vent. The eruption of Nyiragongo volcano in 1997 (Favalli et al., 2006; Tazieff, 1977) had effusion rates alike to the ones obtained for the 1823 eruption, however the volcanic edifice and the type of eruption are not similar to the Great Crack structure. Thus, the Great Crack eruption and its Keaīwa lava flow is a unique scenario where the effusion rates overpassed other big eruptions worldwide in a short timeframe.

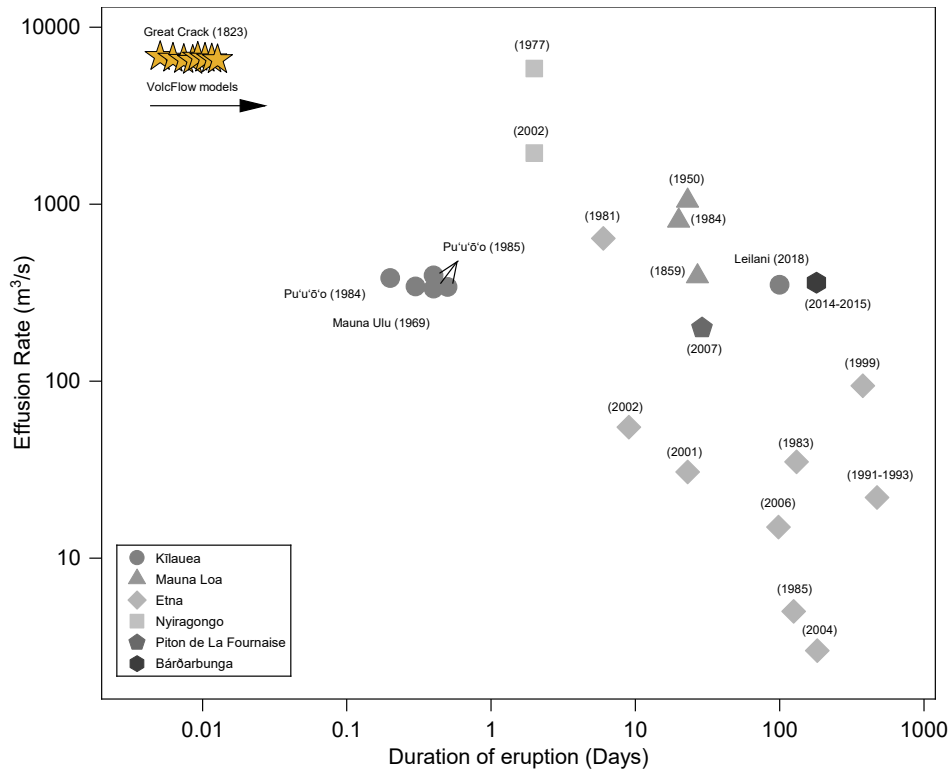


Fig. 15. The plot shows a comparison between the VolcFlow model results and other eruptions that occurred worldwide in terms of effusion rate vs time. The black arrow shows the tendency of the VolcFlow models in time. Eruption rates shown for comparison are from (Aocella & Neri, 2009; Andronico & Lodato, 2005; Calvari et al., 1994; Coltelli et al., 2007; Coppola et al., 2017; Dietterich et al., 2021; Favalli et al., 2006; Harris & Neri, 2002; Lipman & Banks, 1987; Staudacher et al., 2009; Tazieff, 1977; Vicari et al., 2007)

Discussion

Formation of the Great Crack

The Great Crack is one of many ground cracks documented within a 3 km-wide belt the SWRZ, many coinciding with eruptive fissures. North, and <500 m uprift of the 1823 CE lava flow, the Great Crack quickly and noticeably becomes a less continuous feature, dispersing into many shallower ground cracks. The Great Crack is unique in that it hosts the 1823 CE lava flow along a ~10 km-long continuous stretch. This is unusual for a Hawaiian fissure eruption of tholeiitic basalt, which tends to occur as multiple distinct en echelon fissures over many kilometers (e.g., 1955 and 2018 lower ERZ eruption; Macdonald and Eaton, 1964; Neal et al, 2019).

The walls of the Great Crack are coated with a thin (few centimeters) veneer of 1823 CE lava along much of its length. Many locations along the walls of the Great Crack contain abundant spherical lava balls coated in 1823 CE lava. These lava balls can reach >2 m in diameter but most are <1 m in diameter. Many coat angular clasts ripped up from previous lava flows exposed within the walls of the Great Crack, however some contain a light, highly vesicular, and glassy pumiceous lava of recycled 1823 CE material. These lava balls were likely formed by pieces of wallrock and recycled juvenile material being transported downflow inside the Great Crack while rotating and acquiring their coating. As they sank the lava balls continued to accrete into spherical masses, and

when they floated up again were caught on the edge of the Great Crack where they are exposed today.

New evidence indicates that the Great Crack opened or widened syn-eruptively during the 1823 CE eruption. A crucial piece of evidence for demonstrating this is that the 1823 CE lava flow shows drain-back features into the Great Crack from the molten core of flow units that was capped by an already cooled and solidified crust. Additionally, some of the wall blocks that spalled from the margins of the Great Crack show drain-back features on both sides of the spalled blocks. This indicates that these blocks, some several tens of meters long by multiple meters across and with overthickened lava flows, were breaking from the margin and slumping down while the flows were still hot. The Great Crack therefore at the very least widened as the 1823 CE lava was erupting.

While the latter evidence does not necessarily indicate that the Great Crack formed entirely syn-eruptively during the 1823 CE eruption, evidence from immediately older lava flows helps to clarify our argument. The Kealaalea Hills erupted sometime between the 1790 CE Keanakāko‘i Tephra unit I and the 1823 CE lava flow (Hazlett et al., 2019), and this lava flow is present on both the eastern and western sides of the Great Crack where it is uprift of and underlies the 1823 CE lava flow (Fig.16). Unlike the 1823 CE lava flow, Kealaalea Hills lava flows display typical pāhoehoe emplacement structures and morphologies indicative of low effusion rate. These lavas are brittlely fractured at the margins of the Great Crack immediately uprift of the 1823 CE lava flow and completely lack drain-back features. Therefore, the Great Crack was not a substantial ground crack when the Kealaalea Hills eruption occurred sometime between 1790–1823 CE.

Additionally, Ellis (1826) in his book stated that residents of Puna district reported that there was a great earthquake around the same time as they reported having seen an eruption in the Southwest Rift Zone. We therefore conclude that the Great Crack unzipped suddenly, and unleashed an outpouring of largely degassed magma without significant overpressure and explosive activity. Without further evidence, it is only possible to speculate as to what caused the unzipping of the Great Crack. This distal subaerial portion of the SWRZ marks the end of the Hilina Fault system, a series of normal listric faults bounding the down dropped southern flank blocks of Kīlauea Volcano (e.g. Denlinger & Morgan, 2014). The opening of the 1823 CE fissure may have occurred subsequent to an important southward flank movement, and may therefore have been tectonically triggered. Such a scenario would be problematic in the context of eruption forecasting because the onset of eruptive activity would not necessarily be preceded by detectable intrusive activity or overpressure in the magmatic system below the SWRZ.



Fig. 16. Great Crack where it breaks the Kealaalea Hills lava flow – erupted less than 33 years prior - that shows no syn-eruptive widening or drain-back features. Also shows that the Great Crack is not as deep in the northern portion as it is down to the southwest.

Magma Source

Geochemical data shows that 1823 CE lavas have a typical rift tholeiitic basalt composition at Kīlauea. Comparisons to other lavas that occurred nearly the same period of time indicate that lavas from the Great Crack have slightly lower MgO and started fractionating plagioclase and clinopyroxene in addition to olivine, without obvious recent input of mafic magma (i.e., olivine Fo is 76-82 on average, close to equilibrium with typical evolved rift magmas). The 1823 CE lava flows are thus unlikely to have originated from the summit magma reservoir shortly prior to eruption. The 1823 lavas are compositionally more similar to the Kealaalea Hills lavas which preceded them by at most three decades. Thus, we suggest that lavas from the Great Crack comes from the leftover of Kealaalea Hills through crystallization.

Emplacement Rate and Lava Flow Velocity

Field observations, such as ramp-up features of 1823 CE lava overtopping tumuli and scoria cones (e.g., Lava Plastered Cones) from previous eruptions, minor spatter, and a lack of pyroclastic material, indicate that the 1823 CE eruption from the Great Crack was emplaced with an unusually high effusion rate and flow velocities. Additionally, many kīpuka formed when the pre-existing topography was overrun by the 1823 CE lava on a relatively gentle topography of $<5^\circ$. This lends support for the 1823 CE lava having been emplaced quickly from its fissure at the Great Crack.

Soule et al. (2003) undertook a comparison of the distribution of surface lava flow morphologies (i.e., pāhoehoe, ‘a‘ā, and transitional) of the July and December 1974 lava flows in addition to the 1823 CE lava flow, which they state has a similar composition, pre-eruptive topography, and eruption temperatures. Their investigation suggested that all of these lava flows were emplaced at similar effusion and flow advance rates of $300 \text{ m}^3/\text{s}$ and $1\text{--}3 \text{ m/s}$, respectively. These are typical Hawaiian tholeiitic basalt eruptions and much lower than previous estimates from the run-up height at the Lava Plastered Cones (Baloga et al., 1995; Guest et al., 1995), which they used to calculate a flow front velocity of 15 m/s and an effusion rate of $21,000 \text{ m}^3/\text{s}$. Soule et al. (2003) calculated velocity from cooling, and obtained a slower flow front velocities of $\sim 6 \text{ m/s}$. They use a measured cooling with distance and an assumed cooling with time. Our VolcFlow modeling results indicate that the 1823 CE lava flow would need a flow front velocity of $\sim 12 \text{ m/s}$ and an effusion rate of $\sim 6,700 \text{ m}^3/\text{s}$ to overtop and cover the parts of the Lava Plastered Cones that we observe in the field (Fig. 11). These velocities are not unusual for channels near active vents (e.g. Lipman and Banks 1987), but highly unusual for flow fronts in Hawai‘i. Hawaiian lava flows can reach high effusion rates as it occurred at Pu‘u‘ō‘o (1985, 1984) and Mauna Ulu (1969), however, these eruptions have occurred in hours to days, and within a short distance from the vent. From modeling, 1823 CE occurred in minutes, and the vent structure is a long continuously fissure of 12 km long. Time and area occupied by this rapid lava flow would represent a catastrophic scenario.

Conclusions

The Keaīwa lava flow erupted from the Great Crack in 1823 in the lower SWRZ, and was the first volcanic event in Hawai‘i in being recorder by westerners in a report published by William Ellis in 1926. This was a unique event of Kīlauea volcano because of its eruptive mechanism and the morphology characteristics of the flow. We propose that this eruption occurred syn-eruptively

with the formation of the Great Crack, evidenced by the presence of a thin layer of 1823 lava that coats the walls of the fissure along much of its length. On the other hand, the Keaīwa flow is an unusual lava flow due to its thin-sheet like morphology, and its very rapid emplacement. This lava flow exhibits a sudden release of non-volatile magma that occupied an almost flat area of $\sim 12 \text{ km}^2$ in a very short time. And, it shows no differences in geochemical composition or unusually high temperatures compared to other Kīlauea eruptions. Despite of this, the 1823 CE lava flow climbed up the pre-existent Plastered Cones, suggesting high effusion rates and velocities of emplacements.

Such unusually behavior in the future would imply a very short time for eruption response. This implies that some tholeiitic basalt eruptions from Kīlauea and Mauna Loa volcanoes can have the majority of their flow fields emplaced in a matter of minutes to hours.

Acknowledgements

We appreciate thoughtful reviews by Drew Downs. We greatly appreciate Hawai'i Volcanoes National Park for providing a research permit (HAVO-2021- SCI-0047) to Drew that supported this work. A. Tonato received support through the National Science Foundation intern program to spend 6 months with the U.S. Geological Survey's Hawaiian Volcano Observatory. Any use of trade, product, or firm names is for descriptive purposes only and does not imply endorsement by the U.S. Government.

CHAPTER 2

Analog models to promote Geosciences in the Hawaiian Islands

Andrea Tonato¹, Tom Shea¹

¹SOEST, University of Hawai‘i at Mānoa, Honolulu HI, USA

Introduction

Geosciences involve topics and processes that can be hard to comprehend and visualize within our human time and spatial scales. These include plate tectonics motion, earthquakes, magmatism, and metamorphism, among others. Geological processes occur over all timescales, from building of new vents and lavas within hours to months, to over thousands or even millions of years (e.g., The formation of the Hawaiian Islands that may last 4 to 6 million years)(HVO, n.d.). It thus can be complex to visualize how geological processes evolve through time, and what were the intermediate steps to form current landscapes. Geoscience educators continuously look for techniques or methodologies that can help students conceptualize better geologic phenomena. Verbal descriptions are generally effective at explaining methodologies, and instructions. Visual representations, on the other hand, help to translate difficult verbal descriptions into comprehensible visual images (Libarkin & Brick, 2002). However, students have different level of cognitive skills when talking about spatial visualization. Some studies thus suggest that a combination of observation and hands-on interaction help students to construct a mental imagery of unfamiliar geometry or spatial domain (Kastens, 2010; Smith, 2001). Therefore, representing geological processes through analog models or experiments can enhance students learning in a fun an easy way. In this project, I focus on teaching dike propagation and caldera collapse using analog models that enable local students to connect geological processes with their surrounding landscapes and environment. These processes are common to all volcanoes that form the Hawaiian Islands and have occurred throughout most of their eruptive history. Although the efforts described here still require a significant amount of testing in classroom environments, qualitative assessment, and verbal feedback is thus far encouraging.

Dike Propagation

A dike is a tabular or sheet-like body of magma that intrudes into the crust (through small existent cracks, or along the areas of lowest stress) until they get to the surface, and then they cool (Fig. 17A). Fine-grained intrusive dikes are usually more resistant to weathering and erosion, which allows them to stand out in nature (Fig.17B).

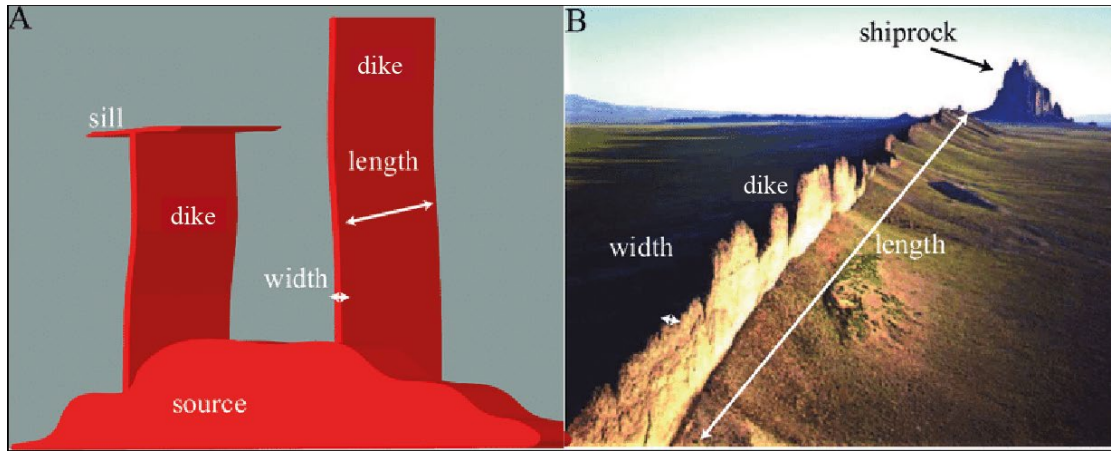


Fig. 17. The image A shows how dike propagates from a source, and B shown how a dike looks like in nature (Taken from Maßmeyer et al., 2013).

Gelatin has been widely used in lab experiments to create a simplified dynamic representation of the Earth's crust. Analog models using gelatin help geologists understand the kinematics and dynamics of shallow crustal processes such as dike propagation, emplacement of laccoliths, and formation of sills (Di Giuseppe et al., 2009; Hyndman & Alt, 1976; Muller et al., 2001; Pansino & Taisne, 2020; Takada, 1990). Although most of these analog models tackle important and complex rheological questions about the behavior of the Earth's crust and enriched our understanding of different rock body emplacements, few studies have focused on leveraging their use for education and outreach to cover the basics of dike propagation under volcanoes.

I propose to apply and improve the techniques and methods used in previous experiments to create a consistent, reproducible dike propagation experiment that will be easy to replicate by whoever is interested in learning and teaching the basic concept of diking. This analog model setup can also be used to develop more complex projects for volcanologists who want to improve our understanding of dike propagation dynamics.

Caldera Collapse

Caldera collapse is a process that deforms the surface of a volcano downwards when the magma chamber empties during and after large eruptions. Eruptions can happen at the summit or when lava breaks through vents or fissures on the sides of the volcano. The volcanic edifice weakens due to the lack of magma in its chamber, the land surface subsides and the area above the shallow magma reservoir collapses (National Park Service, 2023). One example of this process occurred in early May 2018, when the Halema'uma'u crater at the summit of Kīlauea volcano drained as eruptive fissures opened in the lower East Rift Zone (Tepp, 2021). The summit caldera collapsed from mid-May, and continued after the end of the eruption in early August (Fig. 18).



Fig. 18. Caldera collapse during the Pu'u'Ō'o eruption in 2018. Photos show a deformation of the Halema'uma'u crater at the summit of Kīlauea volcano. Photographs belong to the U. S. Geological Survey.

In this project, we built an analog model that replicates the caldera collapse that occurred in 2018 at Kīlauea Volcano. This is an analog model that can be replicated, and carried out to school exhibitions to help students understand about Hawaiian volcanism.

Methods

Dike propagation

To develop this model, we divided our approach in four different stages, design, gelatin preparation, trials, and outreach. We started choosing all the materials (Fig. 19) and selecting the most appropriate dimensions for a glass container. It had to be light-weight, transportable, and as safe as possible in case of brakes.

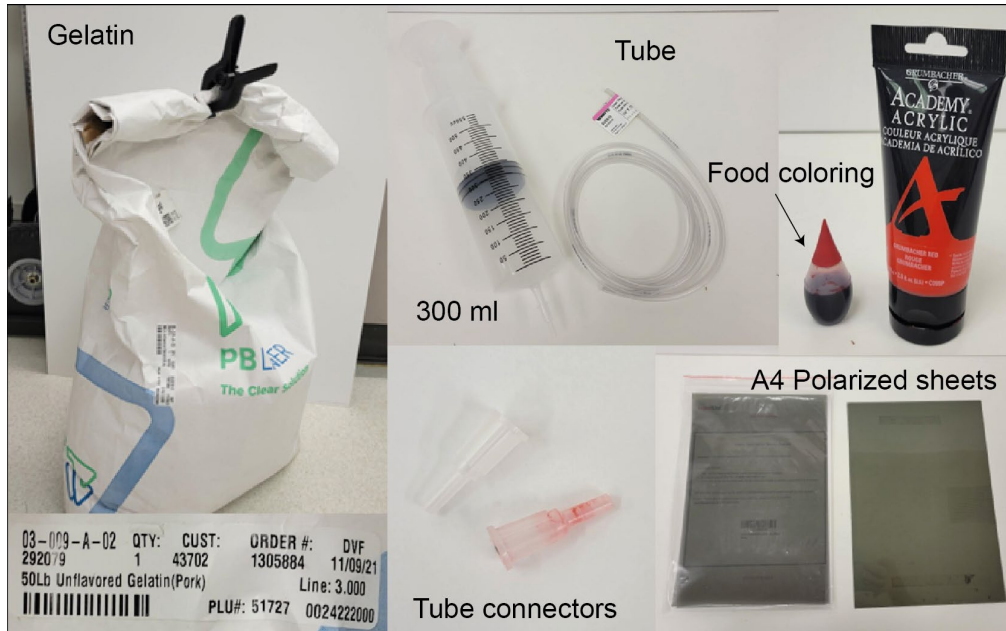


Fig. 19. Main materials used in the setup of the analog model for dike propagation.

We designed the container on Autodesk fusion to have an idea of the length, width and height. Then, we used plexiglass of 0,5 mm thickness to build the tank, it is a strong thermoplastic that has optical clarity, and is resistant and safe to carry. Additionally, it is relatively easy to cut, sand and glue each piece together. This is important as the container will have a tiny whole at its base. The dimensions we suggest to replicate this model are: 30 cm x 18 cm x 21 cm (Fig. 20). This container fits 12 liters of liquid gelatin.

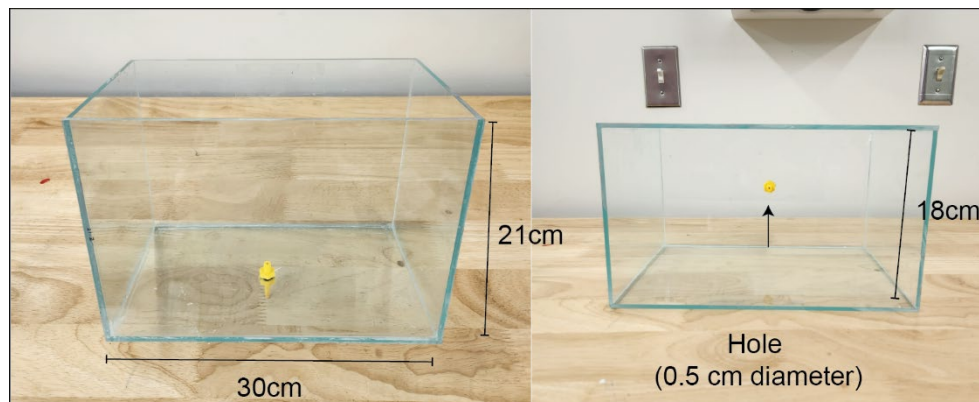


Fig. 20. Dimension of the tank made of plexiglass showing the hole at the base of the container.

We used industrial gelatin at 1.5, 3 and 5 % concentration as suggested in past experiments (Hyndman & Alt, 1976; Muller et al., 2001; Takada, 1990). We also add two caps of bleach to the gelatin mixture to prevent fungus growth. We let the gelatin cool and set at temperatures of 20°C during 24 hours in the plexiglass tank (Fig. 21).

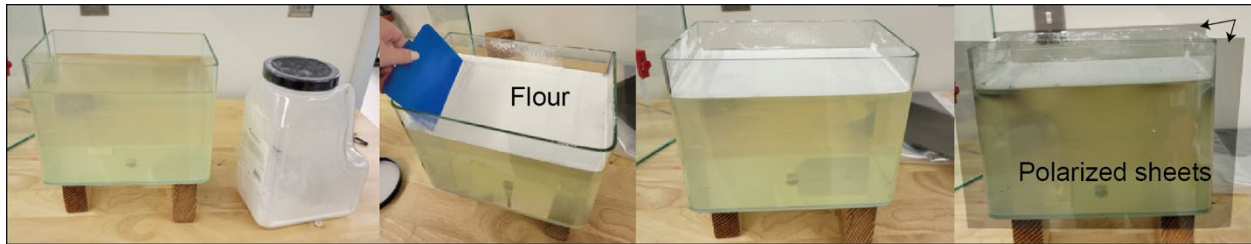


Fig. 21. Gelatin after 24 hours. It shows how to add the layer of flour, and where to place the polarized sheets.

To simulate our magma, we used water and two options of red coloring, food coloring, and acrylic paint. We mixed our color in cold water, and hot water to see the differences when injecting the liquid in the gelatin. For the injection, we used a 300 ml syringe.

Before injecting the water in the gelatin, we created two scenarios: (1) a gelatin with a pre-existing incision of approximately 4 cm long from the bottom to the top of the tank, and (2) a gelatin without the incision.

For extra observations, we also added a thin layer of flour at the top of the gelatin when it was set. When the liquid is being injected, the flour helps to visualize deformation on the top of the gelatin (Fig. 21).

All these experiments were done after placing two polarized sheets on two parallel sides of the glass tank and lights to see the stresses caused by the force when liquid is intruding the gelatin. We took pictures, and filmed the experiments with normal cameras, and with lidar camera, to measure differences in height of the surface. These measurements can therefore be tailored to lab activities at high school and college level.

Caldera Collapse

For these experiments, we designed a triangular tank with a small ramp. We used sand, flour, a ballon, a system of plastic tubes and red water coloring to simulate fissure eruptions and caldera collapse. The tank is also built of plexiglass due to its resistant, safe properties. To create a deformable volcanic edifice we use sand, and covered the top with a thin layer of white flour to improve the observations of the surface deformation. The ballon plays the role of a magma chamber inside the volcano edifice, and the magma inside is represented by water with red coloring. The ramp of the set up is used as the flank of the volcano and has four small water faucets that will allow to drained the magma chamber, as eruptive vents in the rift zone would do. Everything is connected by a system of ¼-in tubes and drip irrigation fittings (Fig. 22).

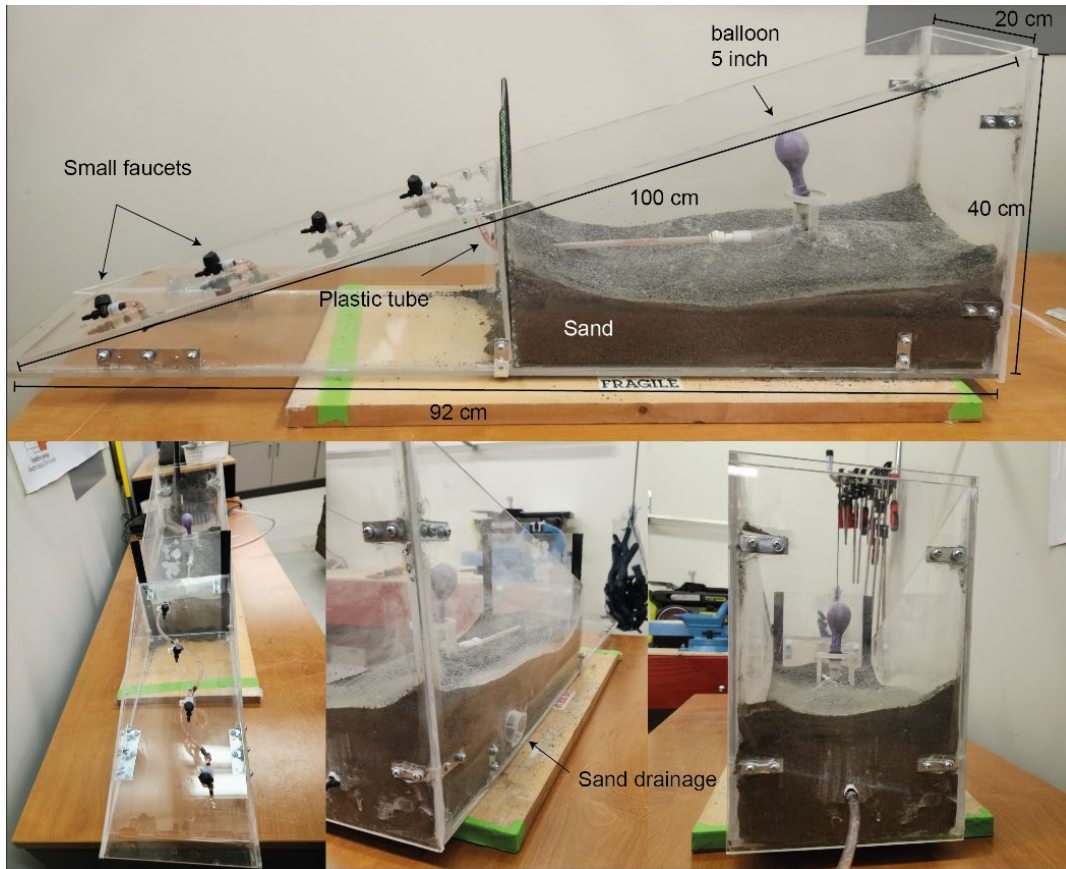


Fig. 22. Image shows dimensions and every item used to build the set up of the caldera collapse model.

Results

Dike Propagation

The gelatin at 5 % concentration was the best option for us, it will be hard gelatin, that wouldn't brake when transporting, and at the same time, it keeps its viscoelastic properties that simulate well the plasticity of the Earth crust. We also colored our gelatin to simulate different layers of strata, however, color diffusion in the gelatin messed all the colors, blocking the clarity of the gelatin when our magma liquid is being injected (Fig. 23). Thus, our best option was transparent gelatin.

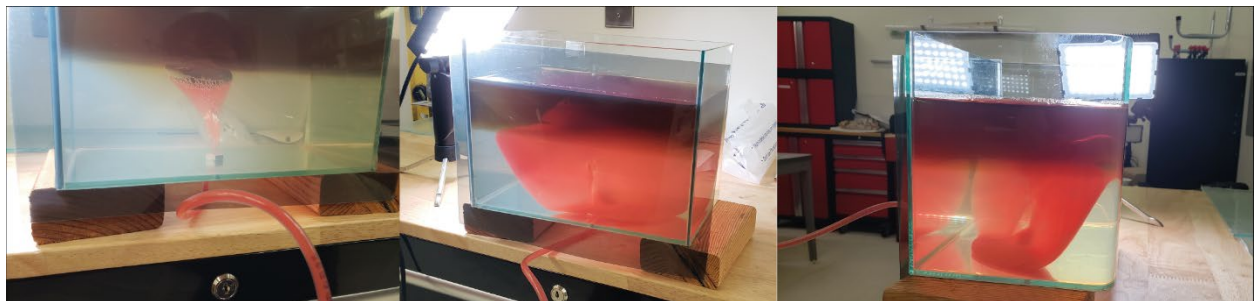


Fig. 23. The set of photos show two layers of gelatin that diffused, and impede to clearly see the intrusion of colored water.

The syringe of 300 mL had the right amount of liquid to create an eruption in a gelatin tank of the suggested dimensions. To simulate magma, we use water and coloring. Food coloring diffuses very well in the water, and keep a transparent touch in the liquid that doesn't leave a strong trace when it is injected in the gelatin. By contrast, acrylic paint changes a little the consistency of the water, and will leave a better trace of the color in the gelatin for observations due to its opacity (Fig. 24). On the other hand, temperature of the water-color mixture will only affect the eruption result. Hot water injection will create a tiny pressure of water vapor while being injected, ending in a tiny eruption with fountaining. No extraordinary observations were made after cold water injection.

A different set of experiments were done by creating a small incision of approximately 4 cm from the bottom to the top of the gelatin. Injecting water without a previous crack in the gelatin will make it brake randomly until it reaches the surface and will cause a normal eruption. Conversely, if we make a crack, we have more control of the direction and reproducibility of the experiment. Therefore, that was the best option for this model. It is an analog model that will be replicated as many times as possible, and that has to be consistently reproducible for teaching purposes.

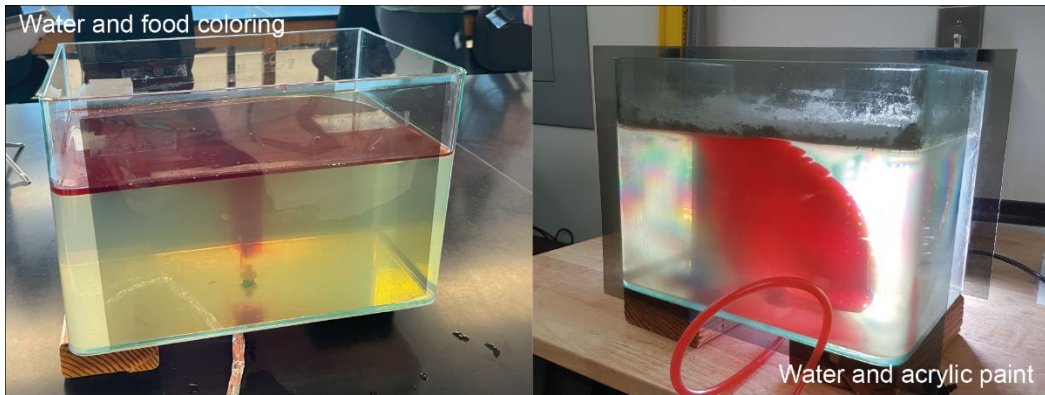


Fig. 24. Differences between using water with food coloring, and water with acrylic paint.

Caldera Collapse

This model results are very visual for all audiences. The setup emulates well the eruptive vents on the flank of the volcano. It is easy to track how the magma chamber drains, how the upper portions of the volcanic edifice weaken, and the progressive formation of a caldera at the top.

A typical model sequence is as follows: First, all the faucets are open until we fill the tube system with magma (water with red coloring), and all the air pressure has gone out of the system (Fig. 25). Then, we close all the faucets, and keep injecting magma. All the water will inflate the balloon, and will instantly show how the surface deforms, and radial cracks form on the flour.



Fig. 25. Sequence of photos show (from left to right) the faucets of the system closed, while red water is being injected creating radial cracks at the summit of the modeled volcano.

The small faucets represent the vents on the flanks of a volcano. When one of the faucets is opened, colored water comes out simulating a lava flow, and the surface starts to cave in, ring faults appear and a caldera structure forms (Fig. 26).

We noticed that the order in which we open the faucets matters. If we open the faucet closest to the summit, it will cause a smaller caldera collapse than opening the lower elevation faucet. This model does a great representation of flank eruptions, and simulates accurately the processes occurring at the summit when eruptions occur at different elevations on the flanks.



Fig. 26. From right to left, the photos show the red water flowing down from the tube system creating a caldera collapse at summit of the volcano.

Conclusion

The analog models for dike propagation and caldera collapse are great simulations of these volcanic processes. We applied these models to different students from three years old children to high schoolers. Each model showed to be visual and entertaining, and complemented very well to videos such as the caldera collapse of Kīlauea volcano in 2018. The analog gelatin dike model results are very colorful and handy for kids, who always wanted to touch the end product. Drawings we received subsequently from the Montessori school allows us to qualitatively measure that our school visit and analog model leaves an important impression in their minds (See Appendix A).

These are analog models that help to understand volcanism of the Hawaiian Islands, and they are easy to replicate. Therefore we started creating an instruction video, and pamphlet about the dike propagation model for schools, teachers, and whoever wants to use the set up to teach (see Appendix B).

Acknowledgments

We acknowledge every teacher and student who open their spaces for us to share these analog models in their institutions. We also appreciate the work done by Mikayla Kauinana, the REU student in 2023, who work on the dike propagation model with us, and made a compilation of all the process.

References cited

- Acocella, V., & Neri, M. (2009). Dike propagation in volcanic edifices: Overview and possible developments. *Tectonophysics*, *471*(1–2), 67–77. <https://doi.org/10.1016/j.tecto.2008.10.002>
- Anderson, K. R., Johanson, I. A., Patrick, M. R., Gu, M., Segall, P., Poland, M. P., Montgomery-Brown, E. K., & Miklius, A. (2019). Magma reservoir failure and the onset of caldera collapse at Kīlauea Volcano in 2018. *Science*, *366*(6470). <https://doi.org/10.1126/science.aaz1822>
- Andronico, D., & Lodato, L. (2005). Effusive activity at Mount Etna volcano (Italy) during the 20th century: A contribution to volcanic hazard assessment. *Natural Hazards*, *36*, 407–443.
- Baldwin, E. ., & Wright, G. . (1907). *Kapapala-Kau, Hawaii: Hawaii Territory Survey, 1 sheet, scale 1:24,000*.
- Baloga, S., Spudis, P. D., & Guest, J. E. (1995). The dynamics of rapidly emplaced terrestrial lava flows and implications for planetary volcanism. *Journal of Geophysical Research: Solid Earth*, *100*(B12), 24509–24519.
- Calvari, S., Coltelli, M., Neri, M., Pompilio, M., & Scribano, V. (1994). The 1991 1993 Etna eruption chronology and lava flow-field evolution. *Acta Vulcanologica*, *4*, 1–14.
- Cashman, K. V., Thornber, C., & Kauahikaua, J. P. (1999). Cooling and crystallization of lava in open channels, and the transition of Pāhoehoe lava to 'A'ā". *Bulletin of Volcanology*, *61*, 306–323. <https://doi.org/10.1007/s004450050299>
- Cassidy, M., Manga, M., Cashman, K., & Bachmann, O. (2018). Controls on explosive-effusive volcanic eruption styles. *Nature Communications*, *9*(1). <https://doi.org/10.1038/s41467-018-05293-3>
- Charbonnier, S. J., Germa, A., Connor, C. B., Gertisser, R., Preece, K., Komorowski, J. C., Lavigne, F., Dixon, T., & Connor, L. (2013). Evaluation of the impact of the 2010 pyroclastic density currents at Merapi volcano from high-resolution satellite imagery, field investigations and numerical simulations. *Journal of Volcanology and Geothermal Research*, *261*, 295–315. <https://doi.org/10.1016/j.jvolgeores.2012.12.021>
- Coan, T. (1868). *Notes on the recent volcanic disturbances of Hawaii*. 89–98.
- Coltelli, M., Proietti, C., Branca, S., Marsella, M., Andronico, D., & Lodato, L. (2007). Analysis of the 2001 lava flow eruption of Mt. Etna from three-dimensional mapping. *Journal of Geophysical Research: Earth Surface*, *112*(F2).
- Coppola, D., Ripepe, M., Laiolo, M., & Cigolini, C. (2017). Modelling satellite-derived magma discharge to explain caldera collapse. *Geology*, *45*(6), 523–526.
- Cordonnier, B., Lev, E., & Garel, F. (2015). *Benchmarking lava-flow models*.
- Denlinger, R. P., & Morgan, J. K. (2014). Instability of Hawaiian Volcanoes. *Characteristics of Hawaiian Volcanoes, U.S. Geological Survey Professional Paper 1801*, 149–176. <http://pubs.usgs.gov/pp/1801/>

- Di Giuseppe, E., Funicello, F., Corbi, F., Ranalli, G., & Mojoli, G. (2009). Gelatins as rock analogs: A systematic study of their rheological and physical properties. *Tectonophysics*, 473(3–4), 391–403. <https://doi.org/10.1016/j.tecto.2009.03.012>
- Dietterich, H. R., Diefenbach, A. K., Soule, S. A., Zoeller, M. H., Patrick, M. P., Major, J. J., & Lundgren, P. R. (2021). Lava effusion rate evolution and erupted volume during the 2018 Kīlauea lower East Rift Zone eruption. *Bulletin of Volcanology*, 83, 1–18.
- Donn, J. . (1901). *Hawaii-Hawaiian Islands: Hawaii Territory Survey, 1 sheet, scale 1:120,000*.
- Donovan, J. J., & Tingle, T. N. (1996). An Improved Mean Atomic Number Background Correction for Quantitative Microanalysis. *Microscopy and Microanalysis*, 2(1), 1–7. <https://doi.org/10.1017/S1431927696210013>
- Downs, D. T., Sas, M., & Hazlett, R. W. (2023). Chemistry and petrography of early 19th century basaltic andesites and basalts from the Kamakai‘a Hills in the Southwest Rift Zone of Kīlauea volcano, Hawai‘i. *Journal of Volcanology and Geothermal Research*, 444(November), 107967. <https://doi.org/10.1016/j.jvolgeores.2023.107967>
- Easton, R. ., & Garcia, M. . (1980). *Petrology of the Hilina Formation, Kīlauea Volcano, Hawai‘i*. 43.
- Ellis, W. (1827). *Narrative of a Tour Through Hawaii: Vol. 2nd Editio*.
- Favalli, M., Chirico, G. D., Papale, P., Pareschi, M. T., Coltelli, M., Lucaya, N., & Boschi, E. (2006). Computer simulations of lava flow paths in the town of Goma, Nyiragongo volcano, Democratic Republic of Congo. *Journal of Geophysical Research: Solid Earth*, 111(B6).
- Finch, R. H. (1940). Engulfment at Kilauea Volcano. *The Volcano Letter*, 470, 1–4.
- Gansecki, C., Lee, R. L., Shea, T., Lundblad, S. P., Hon, K., & Parcheta, C. (2019). The tangled tale of Kīlauea’s 2018 eruption as told by geochemical monitoring. *Science*, 366(6470), eaaz0147.
- Garcia, M. O., Pietruszka, A. J., Norman, M. D., & Rhodes, J. M. (2021). Kīlauea’s Pu ‘u ‘Ō ‘ō Eruption (1983–2018): A synthesis of magmatic processes during a prolonged basaltic event. *Chemical Geology*, 581, 120391.
- Garcia, M. O., Pietruszka, A. J., & Rhodes, J. M. (2003). A petrologic perspective of Kīlauea volcano’s summit magma reservoir. *Journal of Petrology*, 44(12), 2313–2339. <https://doi.org/10.1093/petrology/egg079>
- Garcia, M. O., Pietruszka, A. J., Rhodes, J. M., & Swanson, K. (2000). Magmatic processes during the prolonged Pu‘u‘O‘o eruption of Kilauea Volcano, Hawaii. *Journal of Petrology*, 41(7), 967–990.
- Giordano, D., Russell, J. K., & Dingwell, D. B. (2008). Viscosity of magmatic liquids: a model. *Earth and Planetary Science Letters*, 271(1–4), 123–134.
- Guest, J. E., Spudis, P. D., Greeley, R., Taylor, G. J., & Baloga, S. M. (1995). Emplacement of xenolith nodules in the Kaupulehu lava flow, Hualalai Volcano, Hawaii. *Bulletin of Volcanology*, 57(3), 179–184. <https://doi.org/10.1007/BF00265037>
- Gueugneau, V., Charbonnier, S., Esposti Ongaro, T., de’ Michieli Vitturi, M., Peruzzetto, M., Mangeney, A., Bouchut, F., Patra, A., & Kelfoun, K. (2021). Synthetic benchmarking of concentrated pyroclastic current models. In *Bulletin of Volcanology* (Vol. 83, Issue 11). Springer Berlin Heidelberg. <https://doi.org/10.1007/s00445-021-01491-y>
- Hager, W. H., Castro-Orgaz, O., & Hutter, K. (2019). Correspondence between de Saint-Venant and Boussinesq. 1: Birth of the Shallow–Water Equations. *Comptes Rendus - Mecanique*, 347(9), 632–

662. <https://doi.org/10.1016/j.crme.2019.08.004>

- Harris, A. J. L., & Neri, M. (2002). Volumetric observations during paroxysmal eruptions at Mount Etna: pressurized drainage of a shallow chamber or pulsed supply? *Journal of Volcanology and Geothermal Research*, 116(1–2), 79–95.
- Harris, A. J. L., & Rowland, S. K. (2015). Lava Flows and Rheology. *The Encyclopedia of Volcanoes*, i, 321–342. <https://doi.org/10.1016/B978-0-12-385938-9.00017-1>
- Hazlett, R. W., Orr, T. R., & Lundblad, S. P. (2019a). Undocumented Late 18th- to Early 19th-Century Volcanic Eruptions in the Southwest Rift Zone of Kīlauea Volcano, Hawai‘i. *USGS Scientific Investigations Report*, 5010, 13.
- Hazlett, R. W., Orr, T. R., & Lundblad, S. P. (2019b). Undocumented late 18th- to early 19th-century volcanic eruptions in the southwest rift zone of kilauea volcano, Hawaii. *USGS Scientific Investigations Report*, 2019–5010, 1–13. <https://doi.org/10.3133/sir20195010>
- Holcomb, R. T. (1987). Eruptive history and long-term behavior of Kilauea Volcano (Hawaii). In *US Geological Survey Professional Paper* (Vol. 1350, Issue 1, pp. 261–350).
- Hon, K., Kauahikaua, J., Denlinger, R., & Mackay, K. (1994). Emplacement and inflation of pahoehoe sheet flows: observations and measurements of active lava flows on Kilauea volcano, Hawaii. *Geological Society of America Bulletin*, 106(3), 351–370. [https://doi.org/10.1130/0016-7606\(1994\)106<0351:EAIOPS>2.3.CO;2](https://doi.org/10.1130/0016-7606(1994)106<0351:EAIOPS>2.3.CO;2)
- HVO. (n.d.). *Evolution of Hawaiian Volcanoes*.
- Hyndman, D. W., & Alt, D. (1976). *Square Butte and Shaw Butte of the north- ern Adel Mountains provide well exposed center of the main radial dike swarm . Sisters “ stock ,” approximate Cretaceous sedimentary section including the Eagle Sandstone . Dikes stand at higher eleva- tions close. Hearn.*
- Jochum, K. P., Weis, U., Schwager, B., Stoll, B., Wilson, S. A., Haug, G. H., Andreae, M. O., & Enzweiler, J. (2016). Reference Values Following ISO Guidelines for Frequently Requested Rock Reference Materials. *Geostandards and Geoanalytical Research*, 40(3), 333–350. <https://doi.org/10.1111/j.1751-908X.2015.00392.x>
- Johnson, S. K., Houk, L. L., Feng, J., Houk, R. S., & Johnson, D. C. (1999). Electrochemical Incineration of 4-Chlorophenol and the Identification of Products and Intermediates by Mass Spectrometry. *Environmental Science & Technology*, 33(15), 2638–2644. <https://doi.org/10.1021/es981045r>
- Kastens, K. (2010). Object and spatial visualization in geosciences. *Journal of Geoscience Education*, 58(2), 52–57. <https://doi.org/10.5408/1.3534847>
- Katz, M. G., & Cashman, K. V. (2003). Hawaiian lava flows in the third dimension: Identification and interpretation of pahoehoe and aa distribution in the KP-1 and SOH-4 cores. *Geochemistry, Geophysics, Geosystems*, 4(2). <https://doi.org/10.1029/2001GC000209>
- Kelfoun, K. (2021). *VolcFlow*. Laboratoire Magmas et Volcans. https://lmv.uca.fr/volcflow/#ert_panel1-1
- Kelfoun, K., & Druitt, T. H. (2005). Numerical modeling of the emplacement of Socompa rock avalanche, Chile. *Journal of Geophysical Research: Solid Earth*, 110(12), 1–13. <https://doi.org/10.1029/2005JB003758>
- Kelfoun, K., & Vallejo Vargas, S. (2015). VolcFlow capabilities and potential development for the simulation of lava flows. *Geological Society Special Publication*, 426(1), 337–343.

<https://doi.org/10.1144/SP426.8>

- Libarkin, J. C., & Brick, C. (2002). Research Methodologies in Science Education: Visualization and the Geosciences. *Journal of Geoscience Education*, 50(4), 449–455. <https://doi.org/10.5408/1089-9995-50.4.449>
- Lipman, P. W., & Banks, N. G. (1987). Aa flow dynamics, 1984 Mauna Loa eruption. *U.S. Geol. Surv. Prof. Pap 1350, January 1987*, 1527–1567.
- Lynn, K. J., Garcia, M. O., Shea, T., Costa, F., & Swanson, D. A. (2017). Timescales of mixing and storage for Keanakākoʻi Tephra magmas (1500–1820 C.E.), Kīlauea Volcano, Hawaiʻi. *Contributions to Mineralogy and Petrology*, 172(9). <https://doi.org/10.1007/s00410-017-1395-4>
- Lynn, K. J., & Swanson, D. A. (2022). Olivine and glass chemistry record cycles of plumbing system recovery after summit collapse events at Kīlauea Volcano, Hawaiʻi. *Journal of Volcanology and Geothermal Research*, 426(March), 107540. <https://doi.org/10.1016/j.jvolgeores.2022.107540>
- Macdonald, G. A. (1953). Pahoehoe, aa, and block lava. In *American Journal of Science* (Vol. 251, Issue 3, pp. 169–191). <https://doi.org/10.2475/ajs.251.3.169>
- Macdonald, G., & Eaton, J. P. (1964). *Hawaiian volcanoes during 1955* (Vol. 1171). US Government Printing Office.
- Marquez, M., Paredes, C., & Llorente, M. (2022). Attempt to Model Lava Flow Faster Than Real Time: An Example of La Palma Using VolcFlow. *GeoHazards*, 3(4), 529–563. <https://doi.org/10.3390/geohazards3040027>
- Mattox, T. N., Heliker, C., Kauahikaua, J., & Hon, K. (1993). *Vol6i i)lot 9. 6*, 407–413.
- Muller, J. R., Ito, G., & Martel, S. J. (2001). Effects of volcano loading on dike propagation in an elastic half-space. *Journal of Geophysical Research: Solid Earth*, 106(B6), 11101–11113. <https://doi.org/10.1029/2000jb900461>
- National Park Service. (2023). *Explosive Calderas*. <https://www.nps.gov/articles/000/explosive-calderas.htm#:~:text=Calderas form when magma chambers,the shallow magma reservoir collapses.>
- Neal, C. (2019). *The 2018 rift eruption and summit collapse of Kīlauea Volcano*. 374(January), 367–374.
- Neal, C., & Lockwood, J. (2003). Geologic Map of the Summit Region of Kilauea Volcano, Hawaii. *USGS Geologic Investigations Series I*, 2759(September 1971), 1–15. <papers2://publication/uuid/D8499161-DEBB-496E-AE49-533AD000C961>
- Pansino, S., & Taisne, B. (2020). Shear Wave Measurements of a Gelatin’s Young’s Modulus. *Frontiers in Earth Science*, 8(May), 1–13. <https://doi.org/10.3389/feart.2020.00171>
- Phan-Thien, N., & Pham, D. C. (1997). Differential multiphase models for polydispersed suspensions and particulate solids. *Journal of Non-Newtonian Fluid Mechanics*, 72(2–3), 305–318.
- Pietruszka, A. J., & Garcia, M. O. (1999). A rapid fluctuation in the mantle source and melting history of Kilauea Volcano inferred from the geochemistry of its historical summit lavas (1790–1982). *Journal of Petrology*, 40(8), 1321–1342.
- Pietruszka, A. J., Garcia, M. O., & Rhodes, J. M. (2021). Accumulated Puʻu Ōʻō magma fed the voluminous 2018 rift eruption of Kīlauea Volcano: Evidence from lava chemistry. *Bulletin of Volcanology*, 83, 1–18.

- Poland, M. P., Miklius, A., & Montgomery-Brown, E. K. (2014). Magma Supply, Storage, and Transport at Shield-Stage Hawaiian Volcanoes. *U.S. Geological Survey Professional Paper 1801, 2010*, 1–52.
- Rossi, M. J. (1997). Morphology of the 1984 open-channel lava flow at Krafla volcano, northern Iceland. *Geomorphology*, *20*(1–2), 95–112. [https://doi.org/10.1016/s0169-555x\(97\)00007-x](https://doi.org/10.1016/s0169-555x(97)00007-x)
- Rowland, S. K., & Munro, D. C. (1993). *The 1919–1920 eruption of Mauna Iki, Kilauea: chronology, geologic mapping, and magma transport mechanisms*. 190–203.
- Rowland, S. K., & Walker, G. P. L. (1987). Toothpaste lava: Characteristics and origin of a lava structural type transitional between pahoehoe and aa. *Bulletin of Volcanology*, *49*, 631–641. <https://doi.org/10.1007/BF01079968>
- Rowland, S. K., & Walker, G. P. L. (1990). Pahoehoe and aa in Hawaii: volumetric rate controls the lava structure. *Bulletin of Volcanology*, *52*, 615–628. <https://doi.org/10.1007/BF00301212>
- Shea, T., K. Matzen, A., & J. Mourey, A. (2022). Experimental study of Fe–Mg partitioning and zoning during rapid growth of olivine in Hawaiian tholeiites. *Contributions to Mineralogy and Petrology*, *177*(12), 114.
- Sherrod, D. R., Sinton, J. M., Watkins, S. E., Brunt, K. M., & Survey, U. S. G. (2021). *Geologic map of the State of Hawai'i: U.S. Geological Survey Scientific Investigations Map 3143*. <https://pubs.er.usgs.gov/publication/sim3143>
- Smith, G. (2001). Interaction Evokes Reflection: Learning Efficiency in Spatial Visualization. *EdMedia+ Innovate Learning*.
- Soule, S. A., Cashman, K. V., & Kauahikaua, J. P. (2003). Examining flow emplacement through the surface morphology of three rapidly emplaced, solidified lava flows, Kilauea Volcano, Hawai'i. *Bulletin of Volcanology*, *66*(1), 1–14. <https://doi.org/10.1007/s00445-003-0291-0>
- Staudacher, T., Ferrazzini, V., Peltier, A., Kowalski, P., Boissier, P., Catherine, P., Lauret, F., & Massin, F. (2009). The April 2007 eruption and the Dolomieu crater collapse, two major events at Piton de la Fournaise (La Réunion Island, Indian Ocean). *Journal of Volcanology and Geothermal Research*, *184*(1–2), 126–137.
- Stearns, H. T. (1926). The Keaiwa or 1823 Lava Flow from Kilauea Volcano, Hawaii. *The Journal of Geology*, *34*(4), 336–351. <https://doi.org/10.1086/623317>
- Swanson, D. A. (1973). Pahoehoe flows from the 1969-1971 mauna ulu eruption, kilauea volcano, Hawaii. *Bulletin of the Geological Society of America*, *84*(2), 615–626. [https://doi.org/10.1130/0016-7606\(1973\)84<615:PFFTMU>2.0.CO;2](https://doi.org/10.1130/0016-7606(1973)84<615:PFFTMU>2.0.CO;2)
- Swanson, D. A., & Houghton, B. F. (2019). Products, processes, and implications of Keanakāko'i volcanism, Kīlauea Volcano, Hawai'i. In Michael P Poland, M. O. Garcia, V. E. Camp, & A. Grunder (Eds.), *Field Volcanology: A Tribute to the Distinguished Career of Don Swanson* (Vol. 538, p. 0). Geological Society of America. [https://doi.org/10.1130/2018.2538\(07\)](https://doi.org/10.1130/2018.2538(07))
- Swanson, D. A., Weaver, S. J., & Houghton, B. F. (2014). Reconstructing the deadly eruptive events of 1790 CE at Kīlauea Volcano, Hawai'i. *Bulletin of the Geological Society of America*, *127*(3–4), 503–515. <https://doi.org/10.1130/B31116.1>
- Takada, A. (1990). Experimental study on propagation of liquid-filled crack in gelatin: shape and velocity in hydrostatic stress condition. *Journal of Geophysical Research*, *95*(B6), 8471–8481. <https://doi.org/10.1029/JB095iB06p08471>

- Tate, M. T., Janssen, S. E., Lepak, R. F., Flucke, L., & Krabbenhoft, D. P. (2023). National-Scale Assessment of Total Gaseous Mercury Isotopes Across the United States. *Journal of Geophysical Research: Atmospheres*, 128(8), e2022JD038276. <https://doi.org/https://doi.org/10.1029/2022JD038276>
- Tazieff, H. (1977). An exceptional eruption: Mt. Niragongo, Jan. 10 th, 1977. *Bulletin of Volcanology*, 40(3), 189–200.
- Tepp, G. (2021). Material failure and caldera collapse: Insights from the 2018 Kilauea eruption. *Earth and Planetary Science Letters*, 553, 116621. <https://doi.org/10.1016/j.epsl.2020.116621>
- Thornber, C. R., Orr, T. R., Heliker, C., & Hoblitt, R. P. (2015). Petrologic testament to changes in shallow magma storage and transport during 30+ years of recharge and eruption at Kīlauea Volcano, Hawai ‘i. *Hawaiian Volcanoes: From Source to Surface*, 147–188.
- Vicari, A., Alexis, H., Del Negro, C., Coltelli, M., Marsella, M., & Proietti, C. (2007). Modeling of the 2001 lava flow at Etna volcano by a Cellular Automata approach. *Environmental Modelling and Software*, 22(10), 1465–1471. <https://doi.org/10.1016/j.envsoft.2006.10.005>
- Walker, G. P. L. (1999). Volcanic rift zones and their intrusion swarms. *Journal of Volcanology and Geothermal Research*, 94(1–4), 21–34. [https://doi.org/10.1016/S0377-0273\(99\)00096-7](https://doi.org/10.1016/S0377-0273(99)00096-7)
- Wolfe, E. W., & Morris, J. (1996). *Sample data for the geologic map of the island of Hawaii* (Issues 2524-B). US Geological Survey.